Title

The Histone Deacetylase SIRT6 Restrains Transcription Elongation via Promoter-Proximal Pausing.

Journal

Molecular cell, 75(4)

ISSN

1097-2765

Authors

Etchegaray, Jean-Pierre
Zhong, Lei
Li, Catherine
et al.

Publication Date

2019-08-01

DOI

10.1016/j.molcel.2019.06.034

Peer reviewed

Article

Molecular Cell

The Histone Deacetylase SIRT6 Restrains Transcription Elongation via Promoter-Proximal Pausing

Graphical Abstract

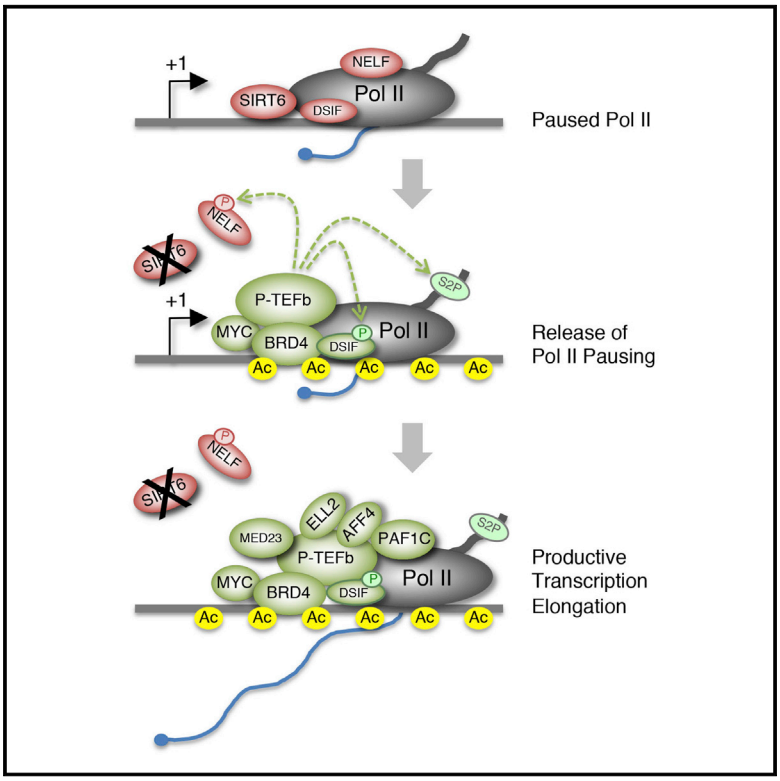

Authors

Jean-Pierre Etchegaray, Lei Zhong, Catherine Li, ..., Karen Adelman, Alon Goren, Raul Mostoslavsky

Correspondence

etchegje@newark.rutgers.edu (J.-P.E.), agoren@ucsd.edu (A.G.), rmostoslavsky@mgh.harvard.edu (R.M.)

In Brief

Historically, histone deacetylases have been described as inhibitors of transcription initiation by compacting chromatin at the transcriptional starting site. Etchegaray et al. identified the histone deacetylase SIRT6 as a critical modulator of transcriptional pausing and elongation, acting downstream of recruitment of Pol II.

Highlights

- The histone deacetylase SIRT6 binds to Pol II and promotes transcriptional pausing
- SIRT6 retains NELF by deacetylating intragenically H3K9 and H3K56
- Removal of SIRT6 from chromatin increases K9/K56 acetylation
- Recruitment of elongation factors promotes transcriptional elongation of SIRT6 targets

Etchegaray et al., 2019, Molecular Cell *75*, 1–17
August 22, 2019
https://doi.org/10.1016/j.molcel.2019.06.034

CellPress

Please cite this article in press as: Etchegaray et al., The Histone Deacetylase SIRT6 Restrains Transcription Elongation via Promoter-Proximal Pausing, Molecular Cell (2019), https://doi.org/10.1016/j.molcel.2019.06.034

Molecular Cell
Article

The Histone Deacetylase SIRT6 Restrains Transcription Elongation via Promoter-Proximal Pausing

Jean-Pierre Etchegaray,[1,11,16,*] Lei Zhong,[1,12,16] Catherine Li,[1,16] Telmo Henriques,[2] Eileen Ablondi,[2] Tomoyoshi Nakadai,[3] Capucine Van Rechem,[1,13] Christina Ferrer,[1] Kenneth N. Ross,[1] Jee-Eun Choi,[1] Ann Samarakkody,[4] Fei Ji,[5,6] Andrew Chang,[1] Ruslan I. Sadreyev,[5,6,7] Sridhar Ramaswamy,[1,14] Sergei Nechaev,[4] Johnathan R. Whetstine,[1,15] Robert G. Roeder,[3] Karen Adelman,[2] Alon Goren,[8,*] and Raul Mostoslavsky[1,9,10,17,*]
[1]The Massachusetts General Hospital Cancer Center, Harvard Medical School, Boston, MA 02114, USA
[2]Department of Biological Chemistry and Molecular Pharmacology, Harvard Medical School, Boston, MA 02115, USA
[3]Laboratory of Biochemistry and Molecular Biology, The Rockefeller University, New York, NY 10065, USA
[4]University of North Dakota School of Medicine, Grand Forks, ND 58201, USA
[5]Department of Molecular Biology, Massachusetts General Hospital, Boston, MA 02114, USA
[6]Department of Genetics, Harvard Medical School, Boston, MA 02115, USA
[7]Department of Pathology, Massachusetts General Hospital, Harvard Medical School, Boston, MA 02114, USA
[8]Department of Medicine, University of California San Diego, La Jolla, CA 92093, USA
[9]The MGH Center for Regenerative Medicine, Harvard Medical School, Boston, MA 02114, USA
[10]The Broad Institute of Harvard and MIT, Cambridge, MA 02142, USA
[11]Present address: Department of Biological Sciences, Rutgers University, Newark, NJ 07102, USA
[12]Present address: Foundation Medicine, Cambridge, MA 02141, USA
[13]Present address: Department of Pathology, Stanford Medicine, Stanford, CA 94305, USA
[14]Present address: Tesaro Inc., Waltham, MA 02451, USA
[15]Present address: Fox Chase Cancer Center, Philadelphia, PA 19111, USA
[16]These authors contributed equally
[17]Lead Contact
*Correspondence: etchegje@newark.rutgers.edu (J.-P.E.), agoren@ucsd.edu (A.G.), rmostoslavsky@mgh.harvard.edu (R.M.)
https://doi.org/10.1016/j.molcel.2019.06.034

SUMMARY

Transcriptional regulation in eukaryotes occurs at promoter-proximal regions wherein transcriptionally engaged RNA polymerase II (Pol II) pauses before proceeding toward productive elongation. The role of chromatin in pausing remains poorly understood. Here, we demonstrate that the histone deacetylase SIRT6 binds to Pol II and prevents the release of the negative elongation factor (NELF), thus stabilizing Pol II promoter-proximal pausing. Genetic depletion of SIRT6 or its chromatin deficiency upon glucose deprivation causes intragenic enrichment of acetylated histone H3 at lysines 9 (H3K9ac) and 56 (H3K56ac), activation of cyclin-dependent kinase 9 (CDK9)—that phosphorylates NELF and the carboxyl terminal domain of Pol II—and enrichment of the positive transcription elongation factors MYC, BRD4, PAF1, and the super elongation factors AFF4 and ELL2. These events lead to increased expression of genes involved in metabolism, protein synthesis, and embryonic development. Our results identified SIRT6 as a Pol II promoter-proximal pausing-dedicated histone deacetylase.

INTRODUCTION

Environmental adaptation is a fundamental trait of all living organisms. Individual cells rely on molecular sensors altering their activities in response to environmental dynamics, such as nutrient availability. The mammalian sirtuin family of proteins (SIRT1-7) are NAD^+-dependent deacetylases capable of sensing changes in nutrient conditions to remodel cellular metabolism (Sebastián et al., 2012a; Choi and Mostoslavsky, 2014; Etchegaray and Mostoslavsky, 2016). SIRT6 is an histone H3K9ac and H3K56 deacetylase, affecting multiple gene networks involved in glucose metabolism, DNA repair, nuclear factor κB (NF-κB) signaling, tumorigenesis, early development, and aging (Kawahara et al., 2009; Michishita et al., 2008, 2009; Yang et al., 2009; Zhong et al., 2010; Sebastián et al., 2012b; Kanfi et al., 2012; Toiber et al., 2013; Kugel and Mostoslavsky, 2014; Silberman et al., 2014; Etchegaray et al., 2015; Kugel et al., 2015, 2016). The deacetylation activity of SIRT6 was also shown to protect telomeric regions from genomic instability (Michishita et al., 2008, 2009) and to promote efficient repair of DNA double-strand breaks (Mao et al., 2011; Toiber et al., 2013). Additionally, SIRT6 can also deacetylate H3K18ac on pericentric chromatin as a potential mechanism to prevent DNA erosion upon cell division during cellular senescence (Tasselli et al., 2016). Our earlier work provided strong evidence for SIRT6 roles in repressing expression of glycolytic, ribosomal, and developmental genes (Sebastián et al., 2012b; Zhong et al., 2010; Etchegaray et al., 2015; Ferrer

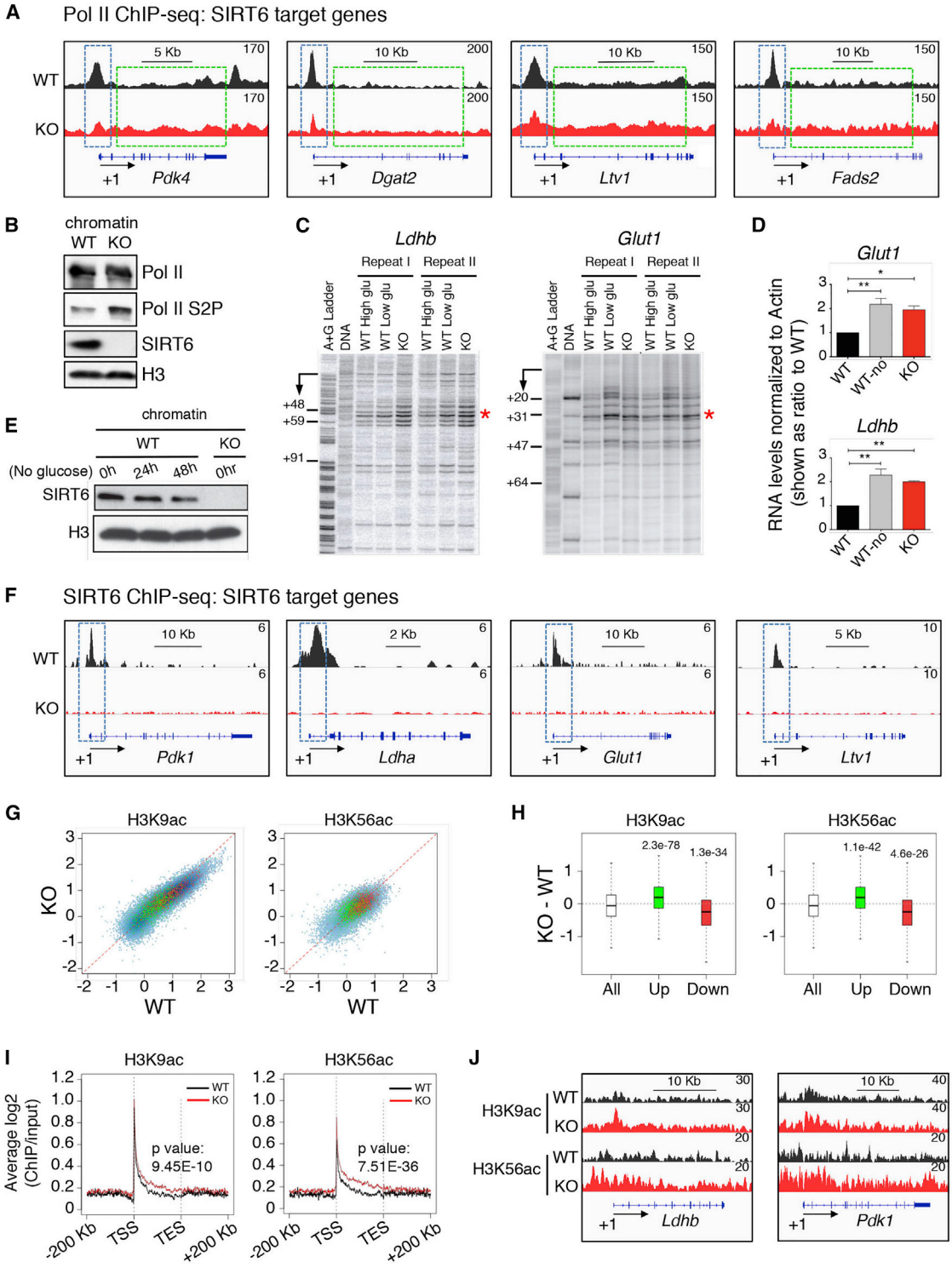

Figure 1. SIRT6 Regulates Transcriptional Pausing via Deacetylation of H3K9ac and H3K56ac

(A) Integrative genomics viewer (IGV) browser (Robinson et al., 2011; Thorvaldsdóttir et al., 2013) images of read coverage across the genome. Images of tiled data files (TDFs) generated by the displaying the density tracks of reads aligned across the genome. The tracks show ChIP-seq maps of Pol II on SIRT6 target genes *Pdk4*, *Dgat2*, *Ltv1*, and *Fads2* in WT (black) and SIRT6 KO (red) ESCs.

(B) Western blots showing levels of Pol II and Pol II Ser2P in the chromatin fraction isolated from WT and SIRT6 KO ESCs.

(legend continued on next page)

et al., 2018). Yet, the specific mechanisms underlying SIRT6-dependent transcriptional silencing remain unclear.

A key regulatory step during transcription occurs during promoter-proximal pausing of RNA polymerase II (Pol II), at ~30–60 nt downstream of the transcription start site (TSS) (Rahl et al., 2010; Bartkowiak et al., 2010; Adelman and Lis, 2012). Pol II pausing is mainly regulated by two pausing-promoting factors, DSIF (DRB-sensitive inducing factor) and NELF (negative elongation factor), which is composed of four subunits (NELF-A, NELF-B, NELF-C/-D, and NELF-E) (Wada et al., 1998; Yamaguchi et al., 1999; Narita et al., 2003; Adelman and Lis, 2012). The release of paused Pol II into productive transcription elongation is facilitated by the recruitment of CDK9-containing P-TEFb (positive transcription elongation factor b), which phosphorylates the C-terminal domain (CTD) of Pol II at serine 2 (Ser2P) as well as the pausing factors resulting in the dissociation of NELF from chromatin and the conversion of DSIF into an elongation-stimulating factor (Marshall et al., 1996; Marshall and Price, 1995; Wei et al., 1998; Fujinaga et al., 2004; Adelman and Lis, 2012; Yamada et al., 2006).

Depending on genetic and cellular contexts, the recruitment of P-TEFb was proposed to be facilitated by c-MYC (MYC), BRD4, as well as different subunits from the Mediator complex including MED23, via interaction with MYC, MED26, and the super elongation complex (SEC) (Rahl and Young, 2014; Liu et al., 2015; Li et al., 2018). BRD4 is a member of the bromodomain and extra-terminal domain (BET) family of transcription factors, which are recruited to acetylated chromatin to promote transcription elongation (Winter et al., 2017). However, the mechanisms downstream of BRD4 that govern release of Pol II pausing into productive elongation remain unclear. Notably, *in vitro* systems using reconstituted chromatinized templates demonstrated that the histone acetyltransferase p300 activity is required for efficient transcription and served to elucidate the role of transcription factors involved in Pol II pausing and elongation (Kim et al., 2010; Pavri et al., 2006).

Acetylation of histones was also shown to stimulate productive transcriptional elongation in live cells (Stasevich et al., 2014). More recently, H3K9ac was shown to release Pol II pausing into transcription elongation by recruiting the SEC complex and thereby loss of H3K9ac caused an increase in Pol II pausing at specific genes in HeLa cells (Gates et al., 2017). These studies indicate that transcriptional pausing could be regulated at the level of chromatin deacetylation. However, the histone deacetylase(s) modulating the transition between transcriptional pausing and productive elongation remained unknown. Here, we show that the histone deacetylase SIRT6 interacts with Pol II and inhibits transcription elongation by decreasing intragenic levels of acetylated H3K9 and H3K56 to modulate recruitment of specific transcription factors. Our results identify SIRT6 as a dedicated chromatin deacetylase for modulating transcriptional pausing and elongation.

RESULTS

SIRT6-Dependent Histone Deacetylation of H3K9ac and H3K56ac Regulate Transcriptional Elongation

To investigate the role of SIRT6 in transcriptional regulation, we performed chromatin immunoprecipitation sequencing (ChIP-seq) analysis in wild type (WT) and SIRT6 knockout (KO) embryonic stem cells (ESCs), using antibodies targeting RNA Pol II (Figure 1A). Notably, we found decreasing levels of Pol II at proximal-promoter sites (dotted blue line square) while increasing amounts within intragenic regions (dotted green line square) on multiple SIRT6 target genes, including *Pdk4*, *Dgat2*, *Ltv1*, and *Fads2* in SIRT6 KO compared to WT ESCs. This differential pattern of gene-loaded Pol II between WT and SIRT6 KO suggested that SIRT6 could influence a transition from a promoter-proximal paused Pol II to an elongating state. The phosphorylation of Pol II within its carboxyl terminal domain at serine 2 (Pol II S2P) is a hallmark for productive transcription elongation (for review, see Jonkers and Lis, 2015). In this context, we found a global increase in the levels of Pol II S2P on chromatin from SIRT6 KO ESCs (Figure 1B).

To further assess roles for SIRT6 in transcriptional regulation, we performed permanganate DNA footprinting, one of the most authoritative means to detect paused polymerase *in vivo* (Nechaev et al., 2010). We analyzed two representative SIRT6 target genes, lactose dehydrogenase b (*Ldhb*) and glucose transporter 1 (*Glut1*) (Figure 1C) (Zhong et al., 2010). We found Pol II pausing on both genes at promoter-proximal regions (between +48 and +59 on *Ldhb* and +31 on *Glut1*) in WT cells. Notably, SIRT6 KO ESCs exhibited a stronger signal within the same regions, showing increased trafficking of Pol II at promoter-proximal sites, indicative of increased transcriptional elongation (Samarakkody et al., 2015). Importantly, increased Pol II trafficking was also observed in WT ESCs grown under glucose deprivation (Figure 1C), demonstrating that SIRT6 deficiency mimics conditions of nutrient stress (Etchegaray and Mostoslavsky, 2016; Zhong et al., 2010). Accordingly, increased mRNA levels for *Ldhb* and *Glut1* were similar both in WT ESCs following glucose deprivation and SIRT6 KO ESCs (Figure 1D), in parallel to the global dissociation of SIRT6 from chromatin following glucose removal from the culturing media (Figure 1E). Using ChIP-seq analysis, we determined that SIRT6 localizes

(C and D) Permanganate footprinting (C) and real-time qPCR (D) showing levels of *Ldhb* and *Glut1* genes in WT ESCs grown in high glucose (black) or no glucose (gray), and SIRT6 KO ESCs (red). Samples were normalized to actin and shown as ratios over WT samples (*$p < 0.05$, **$p < 0.01$, $n > 3$; error bar represents SEM).
(E) Western blots showing levels of SIRT6 and H3 in chromatin fraction from WT ESCs grown in normal glucose (0 h) or under no glucose for 24 h or 48 h and chromatin from SIRT6 KO ESCs grown in normal glucose conditions.
(F) IGV browser images from SIRT6 ChIP-seq showing SIRT6 target genes *Pdk1*, *Ldha*, and *Glut1* and *Ltv1* in WT (black) and in SIRT6 KO ESCs (red).
(G) Scatter plot analysis showing H3K9ac or H3K56ac on upregulated (green) and downregulated (red) genes in SIRT6 KO *versus* WT ESCs. Note that only the upregulated genes exhibit increased signal in the KO cells.
(H) Graphical quantification of the data on (G).
(I) Metagene analysis showing enrichment of H3K9ac or H3K56ac at intragenic regions in SIRT6 KO (red) compared to WT (black) ESCs.
(J) IGV browser images from H3K9ac and H3K56ac ChIP-seq in SIRT6 KO (red) *versus* WT ESCs (black) on *Ldhb* and *Pdk1* genes.

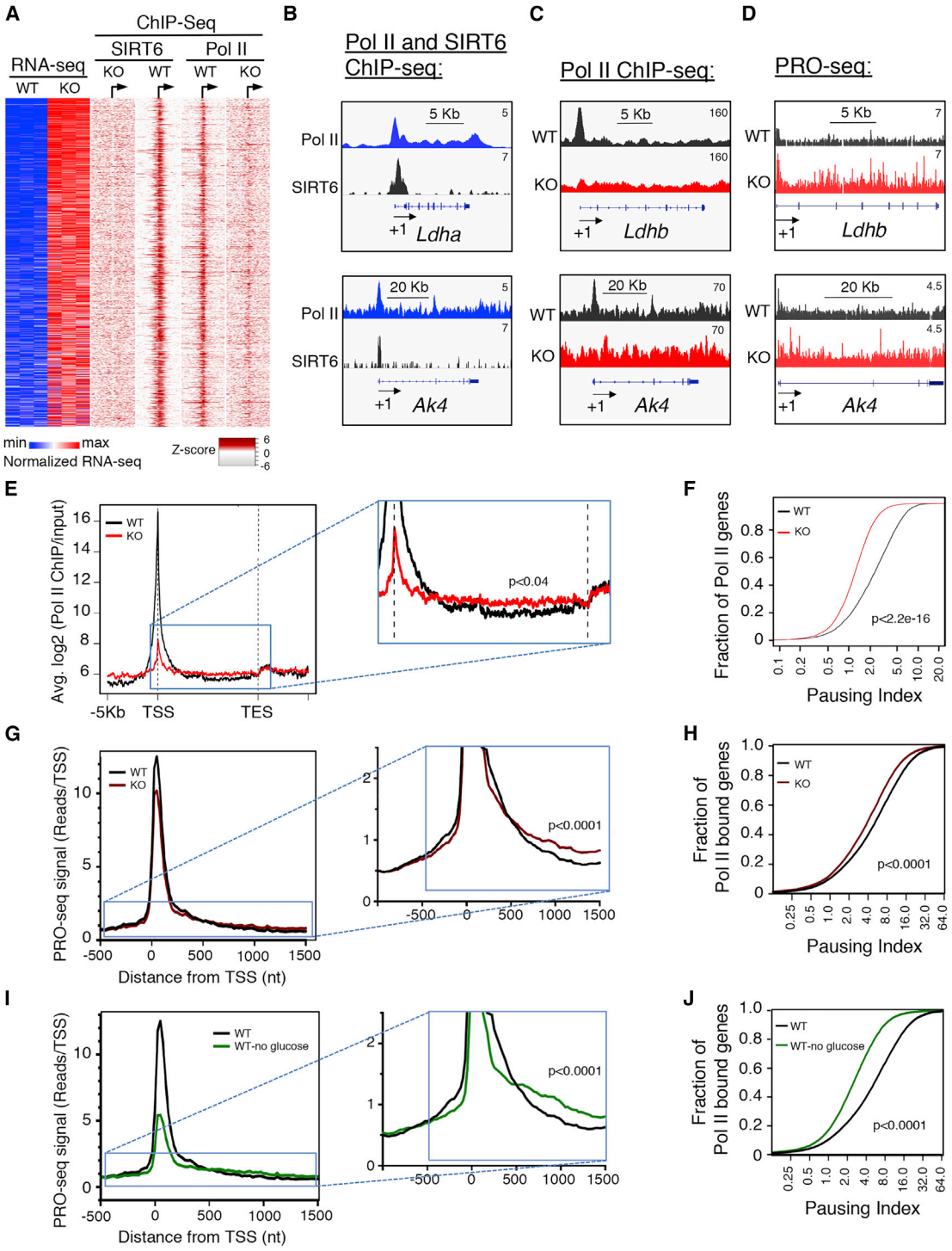

Figure 2. Global Decrease of Pol II Pausing in ESCs Lacking SIRT6

(A) Co-localization of SIRT6 and Pol II. Heatmaps showing Pol II and SIRT6 ChIP-seq signal within 3 kb genomic windows flanking the TSS (the TSS is denoted as an arrow) in WT and SIRT6 KO ESCs. The SIRT6 heatmap on SIRT6 KO ESCs was included as a control.

(B) IGV browser images for of Pol II and SIRT6 ChIP-seq on the SIRT6 target genes *Ldha* and *Ak4*.

(C) IGV browser images from Pol II ChIP-seq showing increased levels on Pol II at intragenic regions (gene bodies) in SIRT6 KO (red) compared to WT ESCs (black) on SIRT6 target genes (*Ldhb* and *Ak4*).

(D) IGV browser images from PRO-seq analysis showing increase levels on Pol II at gene bodies in SIRT6 KO (red) compared to WT ESCs (black) on SIRT6 target genes (*Ldhb* and *Ak4*).

(legend continued on next page)

particularly at promoter-proximal regions of its target genes, including *Pdk1*, *Ldha*, *Glut1*, and *Ltv1* (Figure 1F). Furthermore, by using ChIP-qPCR we also found that SIRT6 binding is lost in WT ESCs cultured under conditions of glucose starvation (Figure S1A). These results support a role for SIRT6 in regulating transcription elongation via Pol II promoter-proximal pausing.

As mentioned above, SIRT6 represses transcription by acting as a specific deacetylase for H3K9ac and H3K56ac (Zhong et al., 2010; Sebastián et al., 2012b; Etchegaray et al., 2015; Kugel et al., 2016). Thus, we performed ChIP-seq experiments in WT and SIRT6 KO ESCs to identify the genomic regions targeted by SIRT6-dependent histone deacetylation impacting gene expression, as determined by RNA sequencing (RNA-seq) analysis (Table S1). RNA- seq identified 4,938 genes upregulated and 4,534 genes downregulated in SIRT6 KO cells. We focused on the upregulated genes, given the likelihood that downregulated genes cannot be explained as direct targets of a deleted histone deacetylase. From the nearly 5,000 genes upregulated in SIRT6 KO ESCs, ~1,200 genes have enriched levels of both H3K9ac and H3K56ac, and ~1,800 genes are enriched for either H3K9ac or H3K56ac (Figure S1B), indicating that most genes upregulated in the SIRT6 KO cells are direct targets of SIRT6. Furthermore, we observed a specific enrichment of these histone marks only on genes that are upregulated in SIRT6 KO ESCs, not the downregulated ones (Figures 1G and 1H; green dots compared to red dots, respectively).

Next, using metagene analysis, we found that the increase in H3K9ac and H3K56ac occurs mainly at promoter-proximal regions and gene bodies (Figures 1I, 1J, and S1C). In addition to metabolism and pluripotency, the genes impacted by SIRT6 removal were also enriched for neural development ontologies (Table S2), which is consistent with the neural-skewed phenotype we observed upon differentiation of SIRT6 KO ESCs (Etchegaray et al., 2015). These results indicate that SIRT6 has a prominent role in modulating histone acetylation within intragenic regions encompassing promoter-proximal pausing and gene bodies. This ability of SIRT6 to regulate intragenic histone acetylation as a potential mean to modulate Pol II pausing and elongation is different from the known roles of class I and class II histone deacetylases (HDACs) that work predominantly at TSS regions, affecting Pol II recruitment at promoter sites (Jones et al., 1998; Nan et al., 1998).

SIRT6 Supports Transcriptional Promoter-Proximal Pausing

To identify the genes mostly affected by SIRT6-dependent Pol II pausing, we first mapped the binding of SIRT6 and Pol II in mouse ESCs in a genome-wide manner. Consistent with the distribution of histone marks, and in contrast to other HDACs (Ram et al., 2011), SIRT6 localized at promoter-proximal pausing sites downstream of the TSS and closely following the positional pattern of Pol II throughout the genome (Figure 2A). Furthermore, when compared to WT, Pol II binding on SIRT6 KO cells exhibits a more diffuse pattern, suggesting increased intragenic binding (Figure 2A). When zoomed in at known SIRT6-targeted genes (Figure 2B-D), a prominent co-localization between Pol II and SIRT6 is observed near promoter-proximal sites. These results indicate that SIRT6 and Pol II are positioned together at the pausing site of these genes.

We next determined whether SIRT6 directly interact with Pol II. Indeed, endogenous SIRT6 co-immunoprecipitated (coIP) with Pol II in WT ESCs, even in the presence of ethidium bromide, indicating that these proteins interact in a direct fashion (Figures S2C–S2E). We further validated this result by mass spectrometry analysis and confirmed interaction of SIRT6 with one of the large subunits of Pol II, RPB2 (Figure S2F), as previously demonstrated by proteomic analysis (Miteva and Cristea, 2014). We next performed metagene analysis of Pol II ChIP-seq data from WT and SIRT6 KO ESCs and identified a significant increase in intragenic signal and a concomitant decrease of promoter-proximal signal for Pol II in SIRT6 KO cells (Figure 2E). Altogether, these results indicate a global role for SIRT6 in inhibiting Pol II transition from promoter-proximal regions to intragenic sites, a transition that is accompanied by active transcriptional elongation.

We next used the Pol II ChIP-seq analysis to calculate pausing index (PI) (Rahl et al., 2010) in WT and SIRT6 KO ESCs cells. Notably, SIRT6 KO cells exhibited a global decrease in PI (Figures 2F and S2G), with over two thousand genes shifted toward an increased productive elongation state. To establish whether these Pol II pausing dynamics correspond to transcriptional changes, we performed a comparative analysis between Pol II ChIP-seq and RNA-seq from WT and SIRT6 KO ESCs (Table S3). Nearly half of the upregulated genes (2,459 out of the 4,938 genes upregulated in SIRT6 KO ESCs, 49.7%) show >2-fold decrease in PI compared to WT ESCs, providing evidence for their regulation by pausing and elongation (Figure S2G). Furthermore, these gene sets showing decreased PI include genes involved in metabolic processes and neural development, consistent with the role of SIRT6 as a key regulator of both metabolism (Kugel and Mostoslavsky, 2014) and early embryonic development (Etchegaray et al., 2015; Ferrer et al., 2018) (Figures S2A and S2B; Table S3).

To confirm these results using an orthogonal approach, we performed precision nuclear run-on sequencing (PRO-seq) analysis (Mahat et al., 2016). PRO-seq identifies nascent RNA in a

(E) Metagene profile, from Pol II ChIP-seq analysis, showing a decrease in Pol II levels near TSS in SIRT6 KO ESCs (red) compared to WT cells (black) and an overall increased intragenic Pol II levels in SIRT6 KO ESCs. Inset: zoom-in of intragenic regions highlighting the higher levels of Pol II in SIRT6 KO cells ($p < 0.04$).
(F) Pausing index, calculated from Pol II ChIP-seq analysis, is decreased in SIRT6 KO compared to WT (gray) ESCs.
(G) Metagene profile, from PRO-seq analysis, showing an overall increased intragenic Pol II levels in SIRT6 KO (red) compared to WT (black) ESCs. Inset: zoom-in of intragenic regions highlighting the higher levels of Pol II in SIRT6 KO cells ($p < 0.0001$).
(H) Pausing index, calculated from PRO-seq analysis, is decreased in SIRT6 KO (red) compared to WT (black) ESCs ($p < 0.0001$).
(I) Metagene profile, from PRO-seq analysis, showing an overall increased intragenic Pol II levels in glucose deprived WT ESCs (green) *versus* WT control cells (black) grown under normal conditions. Inset: zoom-in of intragenic regions highlighting the higher levels of Pol II in glucose deprived WT cells ($p < 0.0001$).
(J) Decreased pausing index, calculated from PRO-seq analysis, in glucose deprived WT ESCs (green) compared to WT control cells (black) ($p < 0.0001$).

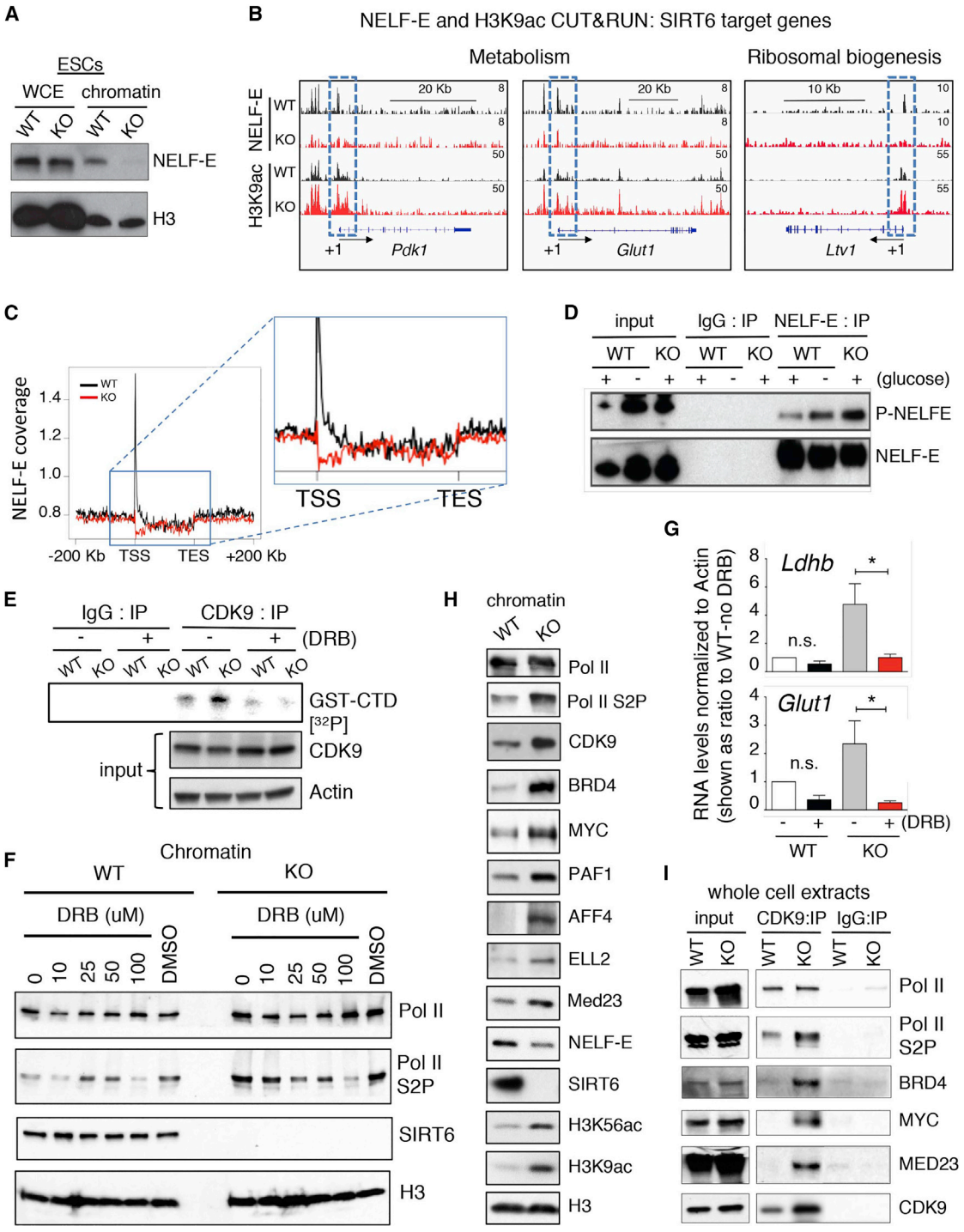

Figure 3. SIRT6 Is an Integral Component of the Pol II Transcription Pausing Machinery

(A) Western blot showing decreased levels of chromatin-bound NELF-E in SIRT6 KO compared to WT ESCs.

(B) IGV browser images from CUT&RUN assays for NELF-E and H3K9ac in WT (black) and SIRT6 KO ESCs (red). TSS regions are denoted as +1 and directionality of transcription by the arrow. Levels of NELF-E and H3K9ac near TSS are highlighted inside the blue dotted line square.

(C) Metagene profile for NELF-E coverage in SIRT6 KO (red) *versus* WT ESCs shows a drastic decrease of NELF-E at promoter-proximal regions.

(D) Phosphorylated NELF-E (P-NELF-E) levels increased in SIRT6 KO and glucose starved WT ESCs compared to WT controls. Western blots showing immunoprecipitation of NELF-E blotted with anti-Phospho-CDK9 substrate and anti-NELF-E antibodies in WT, WT no glucose and SIRT6 KO ESCs.

(legend continued on next page)

way that defines mapping of RNA-Pol II with single base pair resolution, allowing us to evaluate Pol II pausing and elongation in WT versus SIRT6 KO ESCs using an independent approach. Metagene analysis confirmed the decrease Pol II binding at TSS and concomitant increased in signal at gene bodies (Figures 2G and S2I; Table S4). Furthermore, from a total of 3,659 upregulated genes (based on a minimum of 16 reads of Pol II binding; see STAR Methods), and consistent with the Pol II ChIP-seq data analysis described above, we found 2,746 genes (75%) with significantly decreased PI (Figures 2H and S2H). Moreover, this molecular phenotype of decreased PI in SIRT6 KO ESCs was recapitulated in WT ESCs cultured under glucose deprivation (Figures 2I, 2J, and S2I; Table S4). As control for this approach, we found no significant differences in the levels of intragenic Pol II on genes whose expression is unchanged between WT and SIRT6 KO (Figures S2J and S2K). Importantly, between the two methodologies we used to determine PI (Pol II ChIP-seq and PRO-seq), we found an overlapping of 2,022 genes (~80%) that exhibit lower PI in both assays (Table S5). Collectively, using two distinct approaches, we determined that a significant fraction of genes de-repressed in the absence of SIRT6 exhibit decreased transcriptional promoter-proximal pausing, resulting in more Pol II engaged in productive elongation.

SIRT6 Supports Pol II Pausing by Preventing Eviction of NELF-E from Chromatin

Promoter-proximal pausing requires the association of Pol II with the negative transcription elongation factors NELF and DSIF (Kwak and Lis, 2013). Subunits of these negative elongation factors, including NELF-E and SPT5, are phosphorylated by CDK9 (Fujinaga et al., 2004; Jonkers and Lis, 2015; Ping and Rana, 2001). Phosphorylated NELF-E dissociates from chromatin, while SPT5 phosphorylation converts DSIF into a positive elongation factor, leading to productive transcription elongation (Yamada et al., 2006; Gaertner and Zeitlinger, 2014). Given the above results, we next examined whether NELF was altered in SIRT6 KO cells. Strikingly, chromatin levels of NELF-E decreased in SIRT6 KO ESCs (Figure 3A). Similar results were also observed in mouse embryonic fibroblasts (MEFs) derived from SIRT6 KO mice (Figure S3A). Notably, this phenotype can be rescued by expressing a copy of WT SIRT6 (Figure S3A), indicating that the reduction in chromatin-bound NELF-E is dependent on SIRT6. Additionally, binding of NELF-E to chromatin was also gradually diminished upon glucose withdrawal in WT ESCs (Figure S3B).

To specifically investigate NELF binding on SIRT6 target genes, we next performed both CUT&RUN (Skene et al., 2018) and ChIP-qPCR experiments. Indeed, we saw loss of NELF-E at the promoter-proximal regions of SIRT6 target genes in SIRT6 KO ESCs (Figure 3B; note the increased H3K9Ac in the same regions). From ~9,000 genes with lower levels of NELF-E in SIRT6 KO compared to WT ESCs, 1,040 genes have low PI (Figure S3C). Consistently, metagene analysis shows decrease levels of NELF-E in SIRT6 KO ESCs at promoter-proximal regions (Figure 3C; Table S6). We also observed a tight correlation between CUT&RUN and ChIP-seq for H3K9ac, thereby supporting the validity of the CUT&RUN approach (Figure S3D). Additionally, by ChIP-qPCR, we observed decreased levels of NELF-E near promoter-proximal regions, on *Ldhb* and *Glut1* genes in SIRT6 KO ESCs as well as WT cells cultured under glucose deprivation (Figure S3E). These results indicate that chromatin-bound NELF depends on SIRT6 to maintain Pol II promoter-proximal pausing in ESCs.

Because CDK9-dependent phosphorylation is a pre-requisite for the release of NELF-E from chromatin (Fujinaga et al., 2004), we next examined the phosphorylation status of NELF-E in SIRT6 KO *versus* WT ESCs grown under normal or glucose-deprived conditions. Indeed, phosphorylation of NELF-E was increased in both SIRT6 KO ESCs and glucose-depleted WT ESCs, compared to WT ESCs grown under normal nutrient conditions (Figure 3D). These results, together with the increased Pol II phosphorylation we observe in the SIRT6 KO cells (Figure 1B), suggested that eviction or depletion of SIRT6 from its target genes triggers the activation and/or increase recruitment of CDK9. To evaluate this hypothesis, we used an *in vitro* kinase assay and found that CDK9 purified from SIRT6 KO ESCs exhibits increased kinase activity in comparison to CDK9 purified from WT ESCs (Figure 3E). This increased kinase activity is sensitive to the CDK9 inhibitor DRB (5,6-dichloro-1-β-D-ribofuranosyl-1H-benzimidazole). Accordingly, coIP with CDK9 shows increased Pol II Ser2P levels in SIRT6 KO compared to WT ESCs (Figure S3F).

To further confirm that upregulation of SIRT6-targeted genes is CDK9-dependent, we treated ESCs with the CDK9 inhibitor DRB. Efficient inhibition of CDK9 was confirmed by measuring phosphorylation of Pol II (Ser2P) in a dose-dependent manner (Figure 3F). Treatment with DRB rescued the upregulated expression of *Ldhb* and *Glut1* in SIRT6 KO cells (Figure 3G). These experiments indicate that SIRT6 sustains Pol II promoter-proximal pausing by preventing CDK9-dependent phosphorylation of NELF-E and Pol II (Ser2P). Importantly, in addition to the increased activity of CDK9, we observed higher levels of this kinase in the chromatin fraction of SIRT6 KO ESCs (Figure 3H).

Multiple transcription factors were shown to be involved in Pol II pausing release, including MYC (reviewed in Rahl and Young, 2014), the bromodomain protein BRD4 (Yang et al.,

(E) CDK9-dependent *in vitro* kinase assay. CDK9 was immunoprecipitated from either WT or SIRT6 KO ESCs and *in vitro* kinase assay was performed on beads conjugated with a synthetic GST-tagged carboxyl terminal domain of Pol II peptide (GST-CTD) in the presence of ^{32}p-γATP, in the presence or absence of the CDK9 inhibitor DRB. A representative experiment is shown.

(F) Western blot analysis showing decreasing chromatin levels of Pol II S2P by adding the CDK9 inhibitor DRB in a dose-dependent manner to WT and SIRT6 KO ESCs.

(G) Real-time PCR showing levels of *Ldhb* and *Glut1* genes with or without DRB treatment in WT and SIRT6 KO ESCs.

(H) Western blots showing chromatin levels for Pol II, Pol II Ser2P, CDK9, BRD4, MYC, PAF1, AFF4, ELL2, MED23, NELF-E, SIRT6, H3K56ac, H3K9ac, and total histone H3 in WT and SIRT6 KO ESCs.

(I) Western blots showing increased coIP of CDK9 with Pol II Ser2P, BRD4, MYC, and MED23 in SIRT6 KO ESCs.

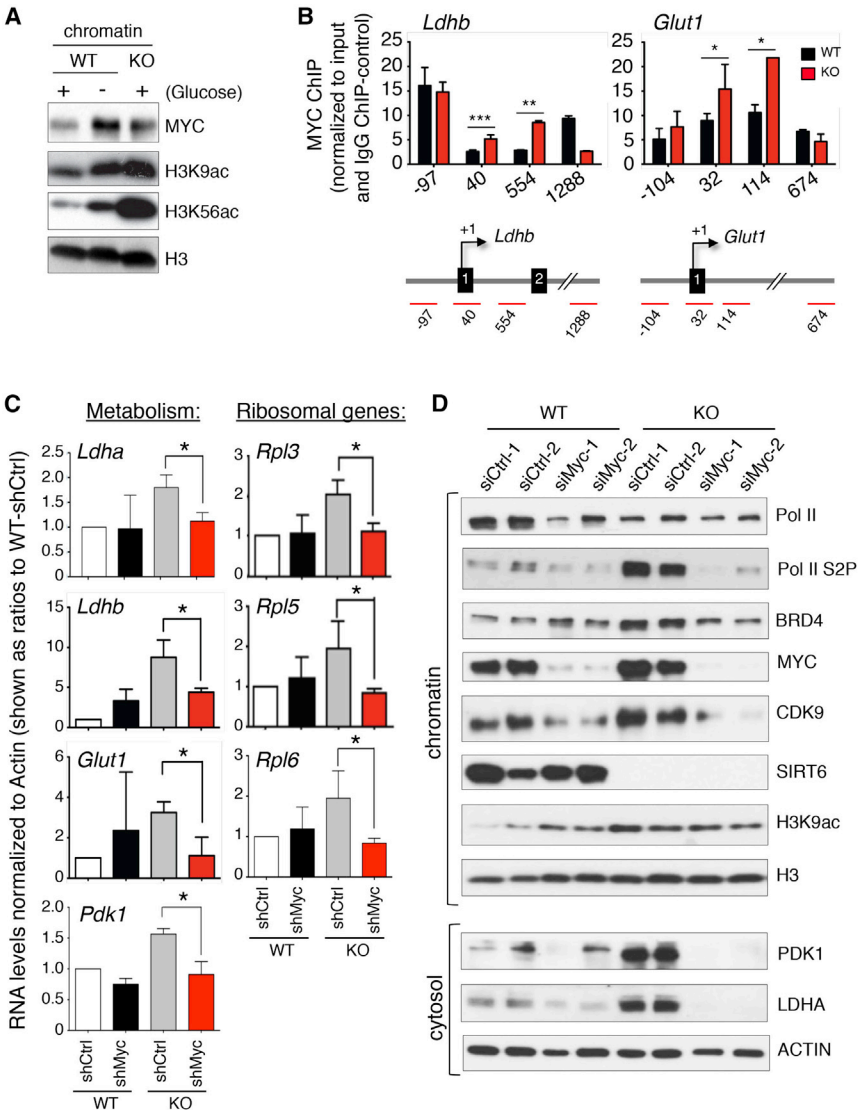

Figure 4. SIRT6 Regulates Transcription by Modulating the Levels of Chromatin-Bound MYC

(A) Western blots showing chromatin bound MYC and levels H3K9ac and H3K56ac in WT, glucose-deprived WT, and SIRT6 KO ESCs.

(B) MYC ChIP-qPCR experiments in *Ldhb* and *Glut1* genes. Schematic representation for these genes are shown below. Samples were normalized to input and further normalized to IgG ChIP controls (*$p < 0.05$, **$p < 0.005$, ***$p < 0.0005$, $n = 3$; error bar represents SEM).

(C) Real-time qPCR analysis showing RNA levels for the metabolic genes *Ldha*, *Ldhb*, *Glut1*, *Pdk1*, and the ribosomal genes *Rpl3*, *Rpl5*, *Rpl6* upon MYC knockdown (shMyc) or a control short hairpin RNA (shRNA) (shCtrl) in WT, glucose-deprived WT, and SIRT6 KO ESCs (*$p < 0.05$, $n = 3$; error bar represents SEM).

(D) Western blot analysis showing decreased Pol II S2P, BRD4, and CDK9 on chromatin of SIRT6 KO ESCs upon acute MYC knockdown using two distinct siRNA oligos. H3 is shown as loading control for chromatin fractions. Cytosolic fractions show the rescue of PDK1 and LDH levels upon acute MYC knockdown in SIRT6 KO ESCs. Actin is included as a loading control.

Increased Transcription Elongation in SIRT6 KO ESCs Is Dependent on MYC, BRD4, and PAF1

MYC has been proposed as a key modulator of transcriptional elongation (Rahl et al., 2010). Following our observation of increased levels of MYC in the chromatin fraction of SIRT6 KO ESCs (Figure 3H), we investigated the role of MYC in the assembly of elongation factors and its effect on gene expression in SIRT6 KO ESCs. We first demonstrate that binding of MYC to chromatin is significantly increased in SIRT6 KO ESCs and in glucose-deprived WT ESCs paralleling the increase in H3K9ac and H3K56ac levels (Figure 4A). Furthermore, ChIP-qPCR experiments demonstrated increased binding of MYC to *Ldhb* and *Glut1* genes in SIRT6 KO ESCs, particularly near promoter-proximal pausing sites (Figure 4B), supporting the known role of MYC as a transcription elongation promoting factor (Rahl et al., 2010). Consistently, MYC knockdown inhibited the expression of various SIRT6-targeted genes, including metabolic and ribosomal protein genes (Figure 4C). MYC deficiency also caused a reduction in CDK9 recruitment and the levels of Pol II (Ser2P), while total Pol II amounts remain unchanged in chromatin from WT and SIRT6 KO ESCs (Figures 4D and S4A). Consistent with the real-time qPCR results, the increase in protein levels of the SIRT6 targets LDHA and PDK1 was fully rescued upon MYC knockdown (Figure 4D, lower panel). Importantly, H3K9 acetylation was not affected by knocking down MYC in SIRT6 KO ESCs, confirming that recruitment of MYC occurs downstream of

2005; Bisgrove et al., 2007; reviewed in Petesch and Lis, 2012), a subunit of the mediator complex, MED23, which has been associated with Pol II transcriptional pause release depending on BRD4 (Wang et al., 2005; Lu et al., 2016), AFF4 and ELL2, which are component of the multi-subunit SEC (Lin et al., 2010; He et al., 2010; Lu et al., 2016), and the Pol II associated factor 1 (PAF1), which is a component of the PAF1 multi-subunit complex (PAF1C) (Van Oss et al., 2017). Strikingly, all of these factors exhibit increased chromatin levels in SIRT6 KO compared to WT ESCs (Figure 3H). Because P-TEFb, which contains CDK9, is recruited to promoter-proximal pausing sites by some of these transcription factors, such as MYC, BRD4, and MED23 (reviewed in Rahl and Young, 2014; Jonkers and Lis, 2015; Lu et al., 2016), we next assessed levels of these factors by coIP with CDK9. Consistently, we find higher levels of BRD4, MYC and MED23 to coIP with CDK9 in SIRT6 KO compared to WT ESCs (Figure 3I), further indicating that SIRT6 inhibits the formation of this multi-protein complex on chromatin.

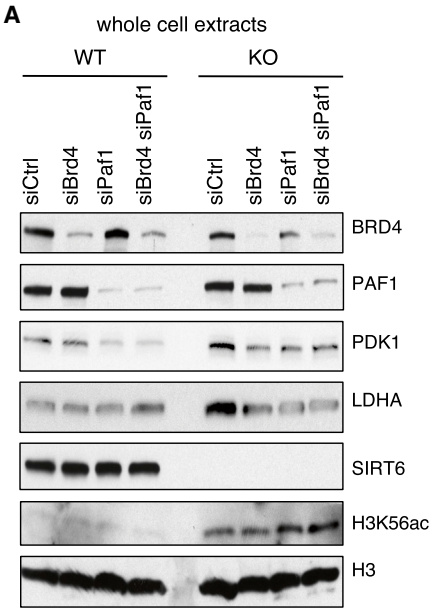

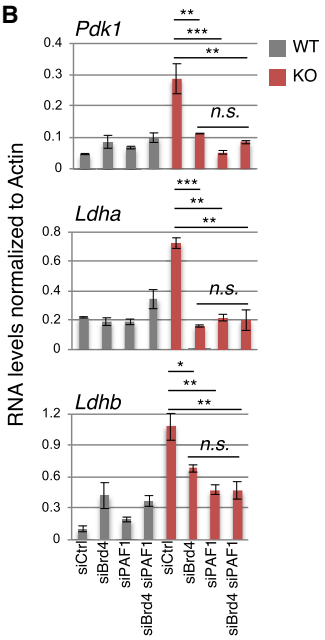

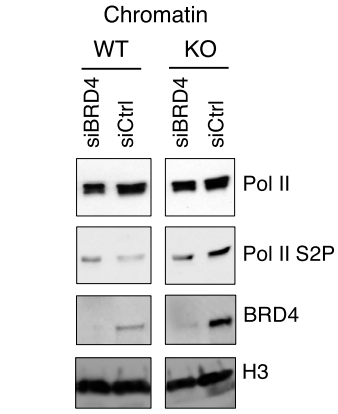

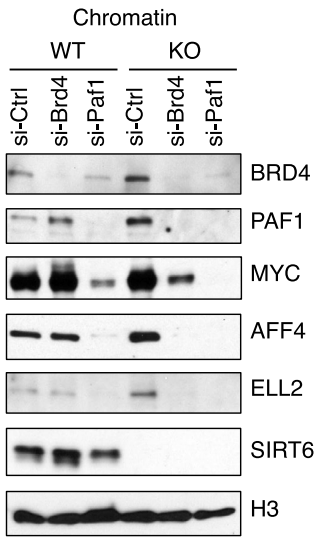

Figure 5. SIRT6 Controls the Assembly of Transcription Elongation and Super Elongation Factors

(A) Western blots from whole cell extracts show levels of PDK1 and LDHA rescued upon acute siRNA-mediated knockdown of BRD4 and/or PAF1 in SIRT6 KO ESCs.

(B) Real-time qPCR analysis showing cDNA levels for *Pdk1*, *Ldha*, and *Ldhb* in WT and SIRT6 KO ESCs following siRNA-mediated knockdown of BRD4 (siBrd4) and/or PAF1 (siPAF1). Samples were normalized to Actin levels (*p < 0.05, **p < 0.01, ***p < 0.001, n = 3; error bar represents SEM).

(C) Western blots showing decreased levels of Pol II Ser2P, in SIRT6 KO ESCs following acute siRNA-dependent BRD4 knockdown (siBRD4).

(D) Western blots showing chromatin levels of BRD4, PAF1, MYC, AFF4, ELL2, SIRT6, and histone H3 in WT and SIRT6 KO ESCs upon acute siRNA-mediated knockdown of BRD4 and/or PAF1.

SIRT6 removal from chromatin and the concomitant increase in histone acetylation (Figure 4D). Together, these results suggest a positive feedback loop between CDK9 and MYC during transcriptional elongation, as previously proposed (Huang et al., 2014).

Given the enrichment of H3K9ac and H3K56ac intragenically (compare SIRT6 KO *versus* WT ESCs) (Figures 1G–1J and S1C), we asked whether readers of these marks may be important in this phenotype. The bromodomain-containing factor BRD4 directly binds acetylated histones and can potentially influence the recruitment of MYC and the activation of CDK9, in turn facilitating transcriptional elongation (Kanno et al., 2014; Yang et al., 2005; Lu et al., 2015; Cheung et al., 2017). Additionally, inhibition of BRD4, using BET inhibitors such as JQ1, was shown to impair ESC self-renewal/pluripotency and to promote cell fate commitment to the neuroectodermal lineage (Di Micco et al., 2014), both phenotypes regulated by SIRT6 (Etchegaray et al., 2015; Ferrer et al., 2018).

We observed an increased recruitment of BRD4 in chromatin from SIRT6-depleted cells (ESCs and MEFs) (Figures 3H and S4B, respectively). Thus, we reasoned that BRD4 may play a role in the release of paused Pol II and tested whether deficiency of BRD4 could rescue gene expression and transcription elongation phenotypes in SIRT6 KO ESCs. While levels of Pol II remain unchanged, small interfering RNA (siRNA)-mediated knockdown of BRD4 reduced Pol II (Ser2P) levels and decreased the expression of SIRT6 targets (*Pdk1*, *Ldha*, and *Ldhb*) (Figures 5A–5D and S4C), indicating a relevant role for BRD4 in SIRT6-dependent regulation of transcription elongation. Moreover, BRD4 knockdown lead to a decrease in chromatin MYC in the absence of SIRT6 (Figure 5D), thus supporting a model for BRD4-dependent recruitment of MYC that triggers the release of paused Pol II into transcription elongation. Notably, WT ESCs appear more resistant to BRD4 knockdown compared to SIRT6 KO ESCs, suggesting that highly acetylated chromatin, due to the absence of SIRT6, is more permissive of BRD4-mediated transcription (Figure 5D).

The PAF1 complex (PAF1C) has been implicated both as a positive (Yu et al., 2015) and negative regulator (Chen et al., 2015) of Pol II pausing release into productive transcription elongation. More recently, comparative three-dimensional studies of paused Pol II and elongating Pol II complexes clearly demonstrated a positive role for PAF1C in facilitating transcription elongation (Vos et al., 2018a; Vos et al., 2018b). Consistent with the

positive role of PAF1C in transcription elongation, we found that upregulation of SIRT6-targets can be rescued by knocking down one of its subunits, PAF1 (Figures 5A and 5B). Furthermore, the recruitment of BRD4 and MYC along with the SEC components AFF4 and ELL2 was severely decreased on chromatin from SIRT6 KO cells upon PAF1 knockdown (Figure 5D). Importantly, knockdown of BRD4 also decreased binding of PAF1, MYC, and the SEC factors (Figure 5D), indicating that both BRD4 and PAF1 may be reinforcing a positive feedback to sustain high levels of these factors on chromatin.

Next, to fully demonstrate a role for PAF1C in the context of SIRT6 regulation, we performed ChIP-seq analysis with an antibody targeting LEO1, a subunit of PAF1C (Van Oss et al., 2017). Consistently, in cells lacking SIRT6, we observed increased binding of LEO1 on multiple SIRT6-target genes, including metabolism, ribosomal biogenesis, neural development, and pluripotency (Figures 6A and S4D; Table S7). The PAF1 complex has also been implicated in facilitating the recruitment of P-TEFb to facilitate phosphorylation of Pol II (Ser2P) (Lu et al., 2016). Indeed, we found that in the absence of SIRT6, the Pol II fraction interacting with different components of the PAF1 complex is highly enriched for Pol II (Ser2P) (Figure 6B). Moreover, higher levels of LEO1 coIP with CDK9 in SIRT6 KO compared to WT ESCs (Figure S4E). Additionally, we found augmented levels of the SEC component AFF4 to coIP with LEO1 and another subunit of the PAF1 complex, CDC73, in SIRT6 KO ESCs (Figure 6B). These results are consistent with previous studies showing that SEC factors can modulate P-TEFb recruitment via interaction with PAF1C (Lu et al., 2016).

Last, by employing ChIP-qPCR, we found an enrichment of the SEC factors ELL2 and AFF4 in SIRT6 KO ESCs specifically at intragenic regions within the SIRT6-target genes *Ldhb* and *Glut1* (Figure 6C). All together, these results indicate that in the absence of SIRT6, both PAF1C and SEC complexes are recruited to chromatin in a coordinated fashion to facilitate transcription elongation of SIRT6-target genes.

SIRT6-Dependent Histone Deacetylation Aligns with H3K36me3 and H3K79me2 Patterns on Genes Involved in Metabolism and Development

Methylation of H3 at lysine 36 (H3K36me3) and 79 (H3K79me2) has been previously associated with active transcriptional elongation (Guenther et al., 2007; Pokholok et al., 2005). We analyzed the genomic levels of these histone modifications in WT *versus* SIRT6 KO ESCs and found that many of the genes whose expression is upregulated in the absence of SIRT6 are enriched for H3K36me3 and/or H3K79me2 (Figure 7A; Table S2). Consistent with our previous studies (Sebastián et al., 2012b; Etchegaray et al., 2015), H3K36me3 and H3K79me2 are enriched at genes involved in metabolic pathways and neural development (Table S2). Although a modest number of genes are enriched for all these epigenetic marks (H3K9ac, H3K56ac, H3K36me3, and H3K79me2) (Figure S5A), a larger number of genes (~300 genes), whose expression is upregulated in SIRT6 KO ESCs, exhibit at least two of these epigenetic marks (Table S2). Plausibly, diverse combinations for these histone marks may be sufficient to trigger transcription elongation in the absence of SIRT6 (see Discussion below).

SIRT6 Depletion Triggers Increased Transcriptional Elongation in an *In Vitro* Assay

To further demonstrate that SIRT6 function as a regulator of Pol II pausing release, we used an *in vitro* transcription elongation assay containing a pre-assembled chromatinized DNA template reconstituted with purified transcription factors from HeLa cells, in the presence of p300/acetyl-CoA, as previously described (Kim et al., 2010). This *in vitro* elongation reaction was supplemented with nuclear extracts from SIRT6 knockdown versus control HeLa cells (Figure 7B). Strikingly, we observed a time-dependent increase of the fully elongated transcript (390 nt) in the presence of the SIRT6-depleted nuclear extract, compared to control (Figures 7C and 7D). Comparable levels of the pre-initiated transcript (17 nt) can be observed with a shorter exposure time (Figure S5B). This *in vitro* transcription elongation approach provides additional evidence that SIRT6 regulates transcription during the transition between pausing and productive elongation.

DISCUSSION

In this study, we demonstrate that SIRT6 is a key regulator of Pol II promoter-proximal pausing. Under normal nutrient conditions, SIRT6 forms a complex with Pol II and maintains histone H3 in a deacetylated state to stabilize Pol II promoter-proximal pausing. Release of SIRT6 from chromatin results in augmented intragenic histone acetylation, thereby facilitating the recruitment of BRD4 and P-TEFb. Beyond increased recruitment of P-TEBb, we observed increased activity of the CDK9 kinase. Notably, the inactive form of CDK9 within the P-TEFb complex, is maintained by its binding to HEXIM1 and the 7SK small nuclear ribonucleoprotein particle (snRNP) RNA (Guo and Price, 2013). However, coIP experiments with CDK9 shows no difference in the levels of HEXIM1 interacting with CDK9 in WT and SIRT6 KO ESCs (Figure S3G), suggesting that the increased activity of CDK9 observed in the KO cells is not dependent on HEXIM1 regulation, but rather may depend on the increased interaction with Pol II and the elongation promoting factors MYC, BRD4, and MED23 (Figure 3I).

This, in turn, causes the phosphorylation and chromatin eviction of NELF-E and the accumulation of Pol II (Ser2P), which facilitates the recruitment of elongation promoting factors including MYC, PAF1, MED23, and the SEC factors AFF4 and ELL2, together leading to the release of Pol II promoter-proximal pausing into productive transcription elongation (Figure 7E). Mechanistically, our results demonstrate that SIRT6-dependent histone deacetylation is critical for maintaining the chromatin landscape in a state that supports Pol II pausing at promoter-proximal regions and prevent productive elongation of target genes. A trigger to inactivate SIRT6 and promote elongation of specific gene sets may depend on cues originated from nutritional changes, developmental stages or proliferation signals.

Although years of research have demonstrated the requirement for histone acetylation in promoting transcription elongation *in vivo* and *in vitro* (Guermah et al., 2006; Kim et al., 2010; Pavri et al., 2006), the specific deacetylase(s) inhibiting transcription elongation at Pol II promoter-proximal pausing sites

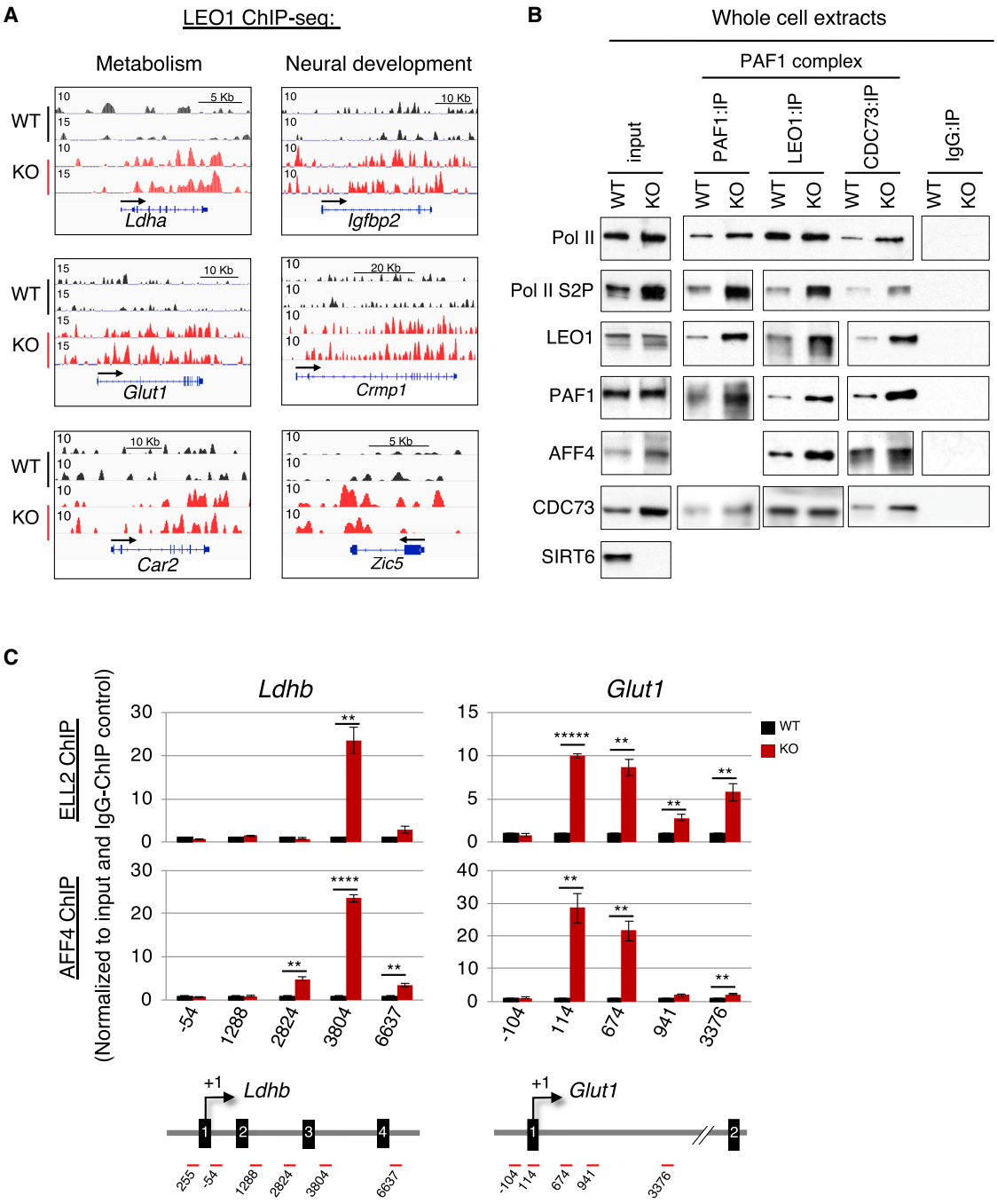

Figure 6. The PAF1 Complex Is a Positive Regulator of Transcription Elongation in ESCs Lacking SIRT6

(A) Increased recruitment of the PAF1C subunit LEO1 in SIRT6 KO ESCs at specific genes. IGV browser images of LEO1 ChIP-seq in SIRT6 KO (red) *versus* WT ESCs (black) on genes implicated in metabolism (*Ldhb*, *Ak4*, *Car2*) and neural development (*Igfbp2*, *Crmp1*, *Zic5*).

(B) Western blot analysis showing increased coIP of PAF1C components PAF1, LEO1, and CDC73 with Pol II, Pol II Ser2P, and the super elongation factor AFF4 in chromatin fractions from SIRT6 KO compared to WT ESCs.

(C) Enrichment of SEC complex at intragenic regions of SIRT6 target genes. ChIP-qPCR analysis of super elongation factors ELL2 and AFF4 at various genomic regions of *Ldhb* and *Glut1* genes, in WT (black) versus SIRT6 KO (red) ESCs. Schematic representation of the *Ldhb* and *Glut1* genes and the location of the regions targeted for qPCR is shown below.

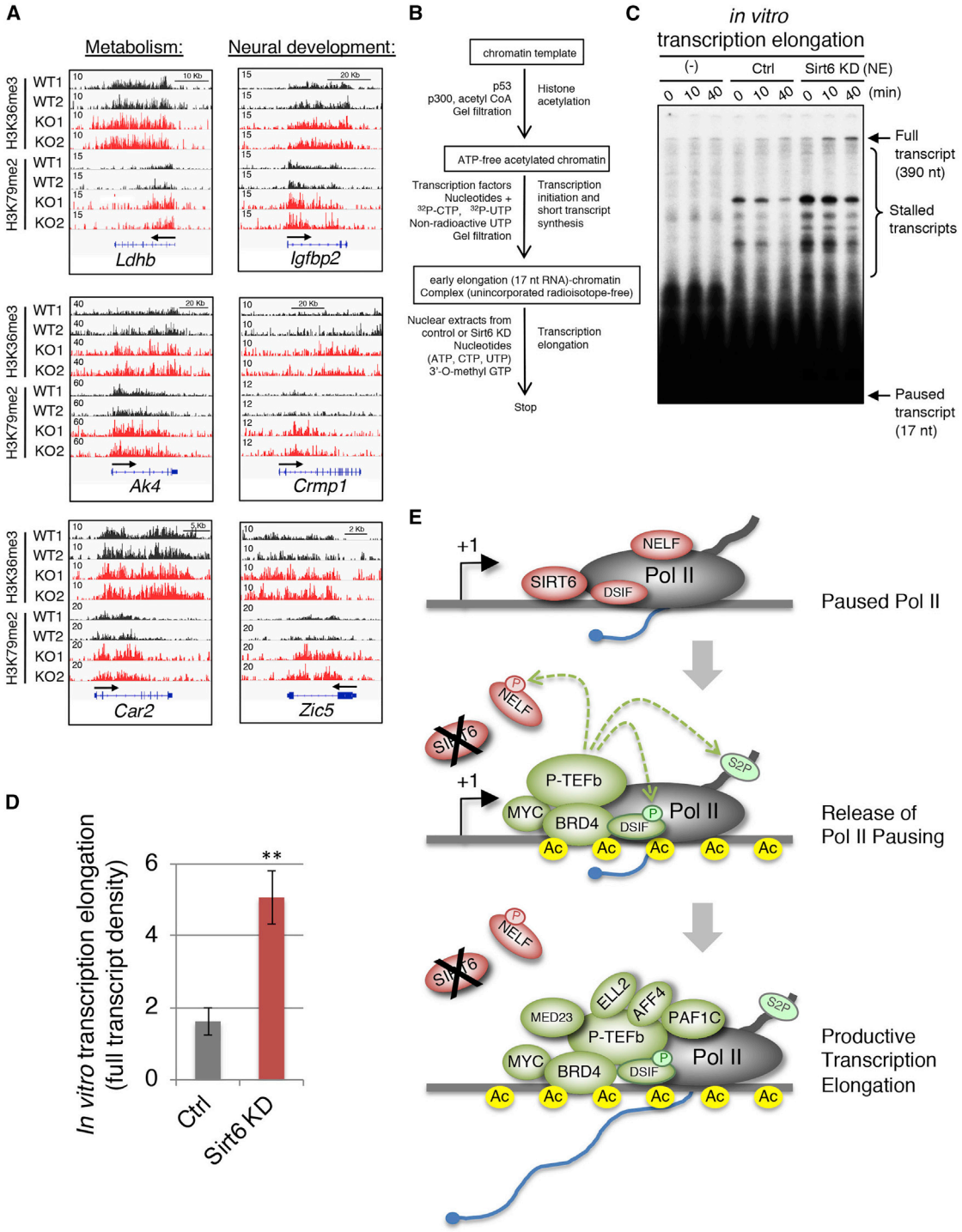

Figure 7. SIRT6-Dependent Chromatin Dynamics Regulates Pol II Elongation

(A) IGV browser images showing the enrichment of H3K36me3 and H3K79me2 on metabolic (*Ldhb*, *Ak4*, *Car2*) and neural developmental (*Igfbp2*, *Crmp1*, *Zic5*) genes in WT (black) and SIRT6 KO (red) ESCs.

(B) Scheme of the *in vitro* transcription elongation protocol using a chromatinized DNA template.

(C) *In vitro* transcription elongation assay showing and augmentation of full elongation capacity in the absence of SIRT6.

(D) Quantification of full elongation products from (C).

(E) Model of SIRT6-dependent regulation of transcription elongation. Under normal nutrient conditions, SIRT6 forms a complex with Pol II at promoter-proximal regions where NELF is retained during transcriptional pausing. In this complex, SIRT6 maintains histone H3 in a deacetylated state on its targeted genes, thereby

(legend continued on next page)

remained unknown. Our studies provide an in-depth mechanistic analysis of a histone deacetylase dedicated to controlling the release of paused Pol II into productive transcription elongation, a function that could confer cells with unique capabilities to fine-tune transcription in response to environmental cues. For instance, dynamic chromatin regulation of Pol II pausing can mediate faster and/or more synchronous modulation of gene expression in response to developmental and nutrient signals. Indeed, transcriptional synchronicity could ensure the orchestration of complex gene regulatory networks controlling mammalian embryogenesis, in accordance to earlier findings demonstrating fine-tuned orderly gene activation patterns in *Drosophila* embryos (Lagha et al., 2013; Boettiger and Levine, 2009). Overall, in the context of ESCs, we propose that this SIRT6-dependent chromatin structure/transcriptional mode may be context-specific. We consider this mechanism to have evolved in order to respond to cellular states and/or environmental cues, via the control of specific gene sets in a robust and synchronous manner. However, our data do not rule out the possibility that SIRT6 might also influence transcription initiation (we saw modest but consistent differences in histone acetylation and Pol II levels at TSS as well), a relevant question that will be addressed in future work. The involvement of other HDAC family members (class I and II) in transcriptional regulation has been shown to be predominantly at the level of gene promoters. For instance, the HDAC1-containing co-repressor complexes N-CoR and Sin3A limit the accessibility of transcription initiation factors to gene promoters (Nagy et al., 1997; Alland et al., 1997; Heinzel et al., 1997). The human NuRD co-repressor complex, containing both HDAC1 and HDAC2, represses transcription by limiting the chromatin access of basal transcription factors to promoter regions (Zhang et al., 1997; Tong et al., 1998; Xue et al., 1998).

The PAF1 complex has been proposed to function as an activator or repressor of transcription elongation depending on genetic/cellular contexts (Van Oss et al., 2017). PAF1 was also found at enhancer regions to restrain transcription on specific gene subsets (Chen et al., 2017). More recently, 3D studies demonstrated that PAF1C functions as a positive transcription elongation factor by displacing NELF from paused Pol II (Vos et al., 2018a, 2018b). Our findings support a role for PAF1C as an activator of transcription elongation, as originally determined in both mouse (Strikoudis et al., 2016) and human ESCs (Yu et al., 2015). Additionally, PAF1C is required for the maintenance of pluripotency in both mouse and human ESCs (Ding et al., 2009; Rigbolt et al., 2011; Ponnusamy et al., 2009). Finally, we demonstrated that levels of PAF1 in chromatin are increased in SIRT6 KO ESCs (Figure 5C), which we have previously showed to have an increased capacity to maintain expression of pluripotency genes (Etchegaray et al., 2015; Ferrer et al., 2018). Thereby, PAF1C might serve as part of a gatekeeper mechanism to uphold the pluripotency state in ESCs by promoting transcription elongation of pluripotency-related genes. In this context, we observed increased interaction of the PAF complex with members of the SEC (Figure 6B) on chromatin, likely due to increase levels of these factors in the absence of SIRT6, further indicating enhanced elongation when SIRT6 is removed from chromatin. Of note, this function of PAF1C might differ upon differentiation, in other cell types or under conditions of disease.

The levels of H3K56ac were shown to correlate with transcription elongation in both yeast and *Drosophila* (Schneider et al., 2006). Thus, the role of H3K56ac as a positive modulator of transcriptional elongation seems to be evolutionary conserved. In addition, it was recently shown that H3K9ac is necessary for the release of paused Pol II by directly recruiting the SEC in HeLa cells (Gates et al., 2017). Removal of SIRT6 from chromatin increases acetylated levels of both H3K9 and H3K56, thereby explaining the enhanced recruitment of SEC components in SIRT6 KO ESCs. In addition, acetylation of histones serves as docking sites for the recruitment of BET bromodomain proteins, such as BRD4, which function as master transcription elongation factors (Winter et al., 2017). Importantly, we found that recruitment of MYC on chromatin is severely impaired upon BRD4 knockdown in the context of SIRT6 depletion, in line with a decreased expression of SIRT6 target genes (Figures 5A, 5B, and 5D). This supports a model where BRD4 is responsible for recruiting MYC onto SIRT6-depleted chromatin to release Pol II pausing. BRD4 was shown to recruit the H3K36 methyltransferase NSD3 to increase gene expression (Rahman et al., 2011; Shen et al., 2015), while MYC interacts with DOT1L, the only known histone methyltransferase to catalyze methylation of H3K79, to induce transcription activation (Cho et al., 2015; Wong et al., 2017). Thus, the enhanced recruitment of BRD4 and MYC to the chromatin fraction that follows the increased levels of H3K9ac and/or H3K56ac upon SIRT6 depletion, may account for the enrichment of H3K36me3 and/or H3K79me2, thereby contributing to the upregulated transcriptional elongation phenotype in SIRT6 KO ESCs. Given our previous studies defining SIRT6 as a co-repressor of MYC in development and cancer (Etchegaray et al., 2015; Kugel et al., 2015, 2016; Sebastián et al., 2012b), our new results indicate that such modulation may depend on the ability of SIRT6 to fine-tune gene expression via transcriptional pausing and elongation to ensure proper cellular differentiation during embryonic development and to protect against malignant transformation.

STAR★METHODS

Detailed methods are provided in the online version of this paper and include the following:

- KEY RESOURCES TABLE
- LEAD CONTACT AND MATERIALS AVAILABILITY

facilitating Pol II pausing. However, under poor nutrient conditions such as glucose starvation, SIRT6 dissociates from the chromatin, allowing acetylation of histone H3, which triggers the recruitment of BRD4 and MYC. This facilitate the recruitment and activation of P-TEFb (containing CDK9), which causes the phosphorylation and chromatin eviction of NELF. Activated P-TEFb also phosphorylates the carboxyl terminal domain of Pol II at serine 2 (Ser2P), which triggers the release of transcriptional pausing. Subsequent recruitment of additional factors including PAF1C, MED23, along with super elongation factors AFF4 and ELL2 impel transcription into productive elongation mode.

SUPPLEMENTAL INFORMATION

Supplemental Information can be found online at https://doi.org/10.1016/j.molcel.2019.06.034.

ACKNOWLEDGMENTS

We would like to thank all the members of the Mostoslavsky lab for helpful discussions. R.M. is the Laurel Schwartz Endowed Chair in Oncology and supported by the Kristin and Bob Higgins Massachusetts General Hospital Research Scholar Award. Antibodies against the SEC complex were kindly provided by Ali Shilatifard. Protein A-MNase and heterologous yeast spike-in DNA for CUT&RUN experiments were kindly provided by Steven Henikoff. This work is supported by NIH (R01GM128448 and R01CA175727 to R.M., R01GM097360 to J.R.W., and R01CA129325 and R01DK071900 to R.G.R.) and the National Science Foundation Graduate Research Fellowship Grant (DGE1745303 to E.F.A.). We would also like to thank the HMS Nascent Transcriptomics Core for support of T.H. and K.A, the Harvard College Office of Undergraduate Research and Fellowships for support of C.L. and A.C., and the Barry Goldwater Scholarship and Excellence in Education Foundation for support of C.L.

AUTHORS CONTRIBUTIONS

J.-P.E. conducted experiments, wrote the manuscript, and participated in the design and interpretation of most of the experiments. L.Z., C.L., E.A., T.N., C.V.R., C.F., J.-E.C., A.S., and A.C. conducted experiments. T.H., K.N.R., F.J., R.I.S., S.R., and K.A. provided all the computational analysis for the different transcriptomics and epigenomic experiments. S.N., J.R.W., R.G.R., and K.A. designed and helped interpreted specific experiments. A.G. designed and coordinated the epigenomic experiments and edited the manuscript. R.M. designed all the experiments, interpreted the data, and wrote the manuscript.

DECLARATION OF INTERESTS

R.M. has a financial interest in Galilei Biosciences Inc., a company developing activators of the mammalian SIRT6 protein. R.M.'s interests were reviewed and are managed by MGH and Partners HealthCare in accordance with their conflict of interest policies. J.R.W. consults for Qsonica and received research funding from Astra Zeneca.

Received: March 26, 2018
Revised: April 11, 2019
Accepted: June 24, 2019
Published: August 6, 2019

SUPPORTING CITATIONS

The following references appear in the Supplemental Information: Thomas et al. (2003).

REFERENCES

Adelman, K., and Lis, J.T. (2012). Promoter-proximal pausing of RNA polymerase II: emerging roles in metazoans. Nat. Rev. Genet. *13*, 720–731.

Alland, L., Muhle, R., Hou, H., Jr., Potes, J., Chin, L., Schreiber-Agus, N., and DePinho, R.A. (1997). Role for N-CoR and histone deacetylase in Sin3-mediated transcriptional repression. Nature *387*, 49–55.

Anders, S., Pyl, P.T., and Huber, W. (2015). HTSeq–a Python framework to work with high-throughput sequencing data. Bioinformatics *31*, 166–169.

Bartkowiak, B., Liu, P., Phatnani, H.P., Fuda, N.J., Cooper, J.J., Price, D.H., Adelman, K., Lis, J.T., and Greenleaf, A.L. (2010). CDK12 is a transcription elongation-associated CTD kinase, the metazoan ortholog of yeast Ctk1. Genes Dev. *24*, 2303–2316.

Bisgrove, D.A., Mahmoudi, T., Henklein, P., and Verdin, E. (2007). Conserved P-TEFb-interacting domain of BRD4 inhibits HIV transcription. Proc. Natl. Acad. Sci. USA *104*, 13690–13695.

Boettiger, A.N., and Levine, M. (2009). Synchronous and stochastic patterns of gene activation in the Drosophila embryo. Science *325*, 471–473.

Chen, F.X., Woodfin, A.R., Gardini, A., Rickels, R.A., Marshall, S.A., Smith, E.R., Shiekhattar, R., and Shilatifard, A. (2015). PAF1, a Molecular Regulator of Promoter-Proximal Pausing by RNA Polymerase II. Cell *162*, 1003–1015.

Chen, F.X., Xie, P., Collings, C.K., Cao, K., Aoi, Y., Marshall, S.A., Rendleman, E.J., Ugarenko, M., Ozark, P.A., Zhang, A., et al. (2017). PAF1 regulation of promoter-proximal pause release via enhancer activation. Science *357*, 1294–1298.

Cheung, K.L., Zhang, F., Jaganathan, A., Sharma, R., Zhang, Q., Konuma, T., Shen, T., Lee, J.Y., Ren, C., Chen, C.H., et al. (2017). Distinct Roles of Brd2 and Brd4 in Potentiating the Transcriptional Program for Th17 Cell Differentiation. Mol. Cell *65*, 1068–1080.

Cho, M.H., Park, J.H., Choi, H.J., Park, M.K., Won, H.Y., Park, Y.J., Lee, C.H., Oh, S.H., Song, Y.S., Kim, H.S., et al. (2015). DOT1L cooperates with the c-Myc-p300 complex to epigenetically derepress CDH1 transcription factors in breast cancer progression. Nat. Commun. *6*, 7821.

Choi, J.E., and Mostoslavsky, R. (2014). Sirtuins, metabolism, and DNA repair. Curr. Opin. Genet. Dev. *26*, 24–32.

Di Micco, R., Fontanals-Cirera, B., Low, V., Ntziachristos, P., Yuen, S.K., Lovell, C.D., Dolgalev, I., Yonekubo, Y., Zhang, G., Rusinova, E., et al. (2014). Control of embryonic stem cell identity by BRD4-dependent transcriptional elongation of super-enhancer-associated pluripotency genes. Cell Rep. *9*, 234–247.

Ding, L., Paszkowski-Rogacz, M., Nitzsche, A., Slabicki, M.M., Heninger, A.K., de Vries, I., Kittler, R., Junqueira, M., Shevchenko, A., Schulz, H., et al. (2009).

A genome-scale RNAi screen for Oct4 modulators defines a role of the Paf1 complex for embryonic stem cell identity. Cell Stem Cell *4*, 403–415.

Etchegaray, J.P., and Mostoslavsky, R. (2016). Interplay between Metabolism and Epigenetics: A Nuclear Adaptation to Environmental Changes. Mol. Cell *62*, 695–711.

Etchegaray, J.P., Chavez, L., Huang, Y., Ross, K.N., Choi, J., Martinez-Pastor, B., Walsh, R.M., Sommer, C.A., Lienhard, M., Gladden, A., et al. (2015). The histone deacetylase SIRT6 controls embryonic stem cell fate via TET-mediated production of 5-hydroxymethylcytosine. Nat. Cell Biol. *17*, 545–557.

Ferrer, C.M., Alders, M., Postma, A.V., Park, S., Klein, M.A., Cetinbas, M., Pajkrt, E., Glas, A., van Koningsbruggen, S., Christoffels, V.M., et al. (2018). An inactivating mutation in the histone deacetylase SIRT6 causes human perinatal lethality. Genes Dev. *32*, 373–388.

Fujinaga, K., Irwin, D., Huang, Y., Taube, R., Kurosu, T., and Peterlin, B.M. (2004). Dynamics of human immunodeficiency virus transcription: P-TEFb phosphorylates RD and dissociates negative effectors from the transactivation response element. Mol. Cell. Biol. *24*, 787–795.

Gaertner, B., and Zeitlinger, J. (2014). RNA polymerase II pausing during development. Development *141*, 1179–1183.

Gates, L.A., Shi, J., Rohira, A.D., Feng, Q., Zhu, B., Bedford, M.T., Sagum, C.A., Jung, S.Y., Qin, J., Tsai, M.J., et al. (2017). Acetylation on histone H3 lysine 9 mediates a switch from transcription initiation to elongation. J. Biol. Chem. *292*, 14456–14472.

Gomes, N.P., Bjerke, G., Llorente, B., Szostek, S.A., Emerson, B.M., and Espinosa, J.M. (2006). Gene-specific requirement for P-TEFb activity and RNA polymerase II phosphorylation within the p53 transcriptional program. Genes Dev. *20*, 601–612.

Guenther, M.G., Levine, S.S., Boyer, L.A., Jaenisch, R., and Young, R.A. (2007). A chromatin landmark and transcription initiation at most promoters in human cells. Cell *130*, 77–88.

Guermah, M., Palhan, V.B., Tackett, A.J., Chait, B.T., and Roeder, R.G. (2006). Synergistic functions of SII and p300 in productive activator-dependent transcription of chromatin templates. Cell *125*, 275–286.

Guo, J., and Price, D.H. (2013). RNA polymerase II transcription elongation control. Chem. Rev. *113*, 8583–8603.

He, N., Liu, M., Hsu, J., Xue, Y., Chou, S., Burlingame, A., Krogan, N.J., Alber, T., and Zhou, Q. (2010). HIV-1 Tat and host AFF4 recruit two transcription elongation factors into a bifunctional complex for coordinated activation of HIV-1 transcription. Mol. Cell *38*, 428–438.

Heinzel, T., Lavinsky, R.M., Mullen, T.M., Söderstrom, M., Laherty, C.D., Torchia, J., Yang, W.M., Brard, G., Ngo, S.D., Davie, J.R., et al. (1997). A complex containing N-CoR, mSin3 and histone deacetylase mediates transcriptional repression. Nature *387*, 43–48.

Henriques, T., and Adelman, K. (2013). Catching the waves: following the leading edge of elongating RNA polymerase II. Mol. Cell *50*, 159–160.

Huang, C.H., Lujambio, A., Zuber, J., Tschaharganeh, D.F., Doran, M.G., Evans, M.J., Kitzing, T., Zhu, N., de Stanchina, E., Sawyers, C.L., et al. (2014). CDK9-mediated transcription elongation is required for MYC addiction in hepatocellular carcinoma. Genes Dev. *28*, 1800–1814.

Jones, P.L., Veenstra, G.J., Wade, P.A., Vermaak, D., Kass, S.U., Landsberger, N., Strouboulis, J., and Wolffe, A.P. (1998). Methylated DNA and MeCP2 recruit histone deacetylase to repress transcription. Nat. Genet. *19*, 187–191.

Jonkers, I., and Lis, J.T. (2015). Getting up to speed with transcription elongation by RNA polymerase II. Nat. Rev. Mol. Cell Biol. *16*, 167–177.

Kanfi, Y., Naiman, S., Amir, G., Peshti, V., Zinman, G., Nahum, L., Bar-Joseph, Z., and Cohen, H.Y. (2012). The sirtuin SIRT6 regulates lifespan in male mice. Nature *483*, 218–221.

Kanno, T., Kanno, Y., LeRoy, G., Campos, E., Sun, H.W., Brooks, S.R., Vahedi, G., Heightman, T.D., Garcia, B.A., Reinberg, D., et al. (2014). BRD4 assists elongation of both coding and enhancer RNAs by interacting with acetylated histones. Nat. Struct. Mol. Biol. *21*, 1047–1057.

Kawahara, T.L.A., Michishita, E., Adler, A.S., Damian, M., Berber, E., Lin, M., McCord, R.A., Ongaigui, K.C.L., Boxer, L.D., Chang, H.Y., and Chua, K.F. (2009). SIRT6 links histone H3 lysine 9 deacetylation to NF-kappaB-dependent gene expression and organismal life span. Cell *136*, 62–74.

Kharchenko, P.V., Tolstorukov, M.Y., and Park, P.J. (2008). Design and analysis of ChIP-seq experiments for DNA-binding proteins. Nat. Biotechnol. *26*, 1351–1359.

Kim, J., Guermah, M., and Roeder, R.G. (2010). The human PAF1 complex acts in chromatin transcription elongation both independently and cooperatively with SII/TFIIS. Cell *140*, 491–503.

Kim, D., Pertea, G., Trapnell, C., Pimentel, H., Kelley, R., and Salzberg, S.L. (2013). TopHat2: accurate alignment of transcriptomes in the presence of insertions, deletions and gene fusions. Genome Biol. *14*, R36.

Kugel, S., and Mostoslavsky, R. (2014). Chromatin and beyond: the multitasking roles for SIRT6. Trends Biochem. Sci. *39*, 72–81.

Kugel, S., Feldman, J.L., Klein, M.A., Silberman, D.M., Sebastián, C., Mermel, C., Dobersch, S., Clark, A.R., Getz, G., Denu, J.M., and Mostoslavsky, R. (2015). Identification of and Molecular Basis for SIRT6 Loss-of-Function Point Mutations in Cancer. Cell Rep. *13*, 479–488.

Kugel, S., Sebastián, C., Fitamant, J., Ross, K.N., Saha, S.K., Jain, E., Gladden, A., Arora, K.S., Kato, Y., Rivera, M.N., et al. (2016). SIRT6 Suppresses Pancreatic Cancer through Control of Lin28b. Cell *165*, 1401–1415.

Kwak, H., and Lis, J.T. (2013). Control of transcriptional elongation. Annu. Rev. Genet. *47*, 483–508.

Lagha, M., Bothma, J.P., Esposito, E., Ng, S., Stefanik, L., Tsui, C., Johnston, J., Chen, K., Gilmour, D.S., Zeitlinger, J., and Levine, M.S. (2013). Paused Pol II coordinates tissue morphogenesis in the Drosophila embryo. Cell *153*, 976–987.

Lee, C., Etchegaray, J.P., Cagampang, F.R., Loudon, A.S., and Reppert, S.M. (2001). Posttranslational mechanisms regulate the mammalian circadian clock. Cell *107*, 855–867.

Li, H., and Durbin, R. (2010). Fast and accurate long-read alignment with Burrows-Wheeler transform. Bioinformatics *26*, 589–595.

Li, Y., Liu, M., Chen, L.F., and Chen, R. (2018). P-TEFb: Finding its ways to release promoter-proximally paused RNA polymerase II. Transcription *9*, 88–94.

Lin, C., Smith, E.R., Takahashi, H., Lai, K.C., Martin-Brown, S., Florens, L., Washburn, M.P., Conaway, J.W., Conaway, R.C., and Shilatifard, A. (2010). AFF4, a component of the ELL/P-TEFb elongation complex and a shared subunit of MLL chimeras, can link transcription elongation to leukemia. Mol. Cell *37*, 429–437.

Liu, X., Kraus, W.L., and Bai, X. (2015). Ready, pause, go: regulation of RNA polymerase II pausing and release by cellular signaling pathways. Trends Biochem. Sci. *40*, 516–525.

Love, M.I., Huber, W., and Anders, S. (2014). Moderated estimation of fold change and dispersion for RNA-seq data with DESeq2. Genome Biol. *15*, 550.

Lu, H., Xue, Y., Yu, G.K., Arias, C., Lin, J., Fong, S., Faure, M., Weisburd, B., Ji, X., Mercier, A., et al. (2015). Compensatory induction of MYC expression by sustained CDK9 inhibition via a BRD4-dependent mechanism. eLife *4*, e06535.

Lu, X., Zhu, X., Li, Y., Liu, M., Yu, B., Wang, Y., Rao, M., Yang, H., Zhou, K., Wang, Y., et al. (2016). Multiple P-TEFbs cooperatively regulate the release of promoter-proximally paused RNA polymerase II. Nucleic Acids Res. *44*, 6853–6867.

Mahat, D.B., Kwak, H., Booth, G.T., Jonkers, I.H., Danko, C.G., Patel, R.K., Waters, C.T., Munson, K., Core, L.J., and Lis, J.T. (2016). Base-pair-resolution genome-wide mapping of active RNA polymerases using precision nuclear run-on (PRO-seq). Nat. Protoc. *11*, 1455–1476.

Mao, Z., Hine, C., Tian, X., Van Meter, M., Au, M., Vaidya, A., Seluanov, A., and Gorbunova, V. (2011). SIRT6 promotes DNA repair under stress by activating PARP1. Science *332*, 1443–1446.

Marshall, N.F., and Price, D.H. (1995). Purification of P-TEFb, a transcription factor required for the transition into productive elongation. J. Biol. Chem. *270*, 12335–12338.

Marshall, N.F., Peng, J., Xie, Z., and Price, D.H. (1996). Control of RNA polymerase II elongation potential by a novel carboxyl-terminal domain kinase. J. Biol. Chem. *271*, 27176–27183.

Maxam, A.M., and Gilbert, W. (1977). A new method for sequencing DNA. Proc. Natl. Acad. Sci. USA *74*, 560–564.

Michishita, E., McCord, R.A., Berber, E., Kioi, M., Padilla-Nash, H., Damian, M., Cheung, P., Kusumoto, R., Kawahara, T.L., Barrett, J.C., et al. (2008). SIRT6 is a histone H3 lysine 9 deacetylase that modulates telomeric chromatin. Nature *452*, 492–496.

Michishita, E., McCord, R.A., Boxer, L.D., Barber, M.F., Hong, T., Gozani, O., and Chua, K.F. (2009). Cell cycle-dependent deacetylation of telomeric histone H3 lysine K56 by human SIRT6. Cell Cycle *8*, 2664–2666.

Mishra, S., Van Rechem, C., Pal, S., Clarke, T.L., Chakraborty, D., Mahan, S.D., Black, J.C., Murphy, S.E., Lawrence, M.S., Daniels, D.L., et al. (2018). Cross-talk between Lysine-Modifying Enzymes Controls Site-Specific DNA Amplifications. Cell *174*, 803–817.

Miteva, Y.V., and Cristea, I.M. (2014). A proteomic perspective of Sirtuin 6 (SIRT6) phosphorylation and interactions and their dependence on its catalytic activity. Mol. Cell. Proteomics *13*, 168–183.

Mostoslavsky, R., Chua, K.F., Lombard, D.B., Pang, W.W., Fischer, M.R., Gellon, L., Liu, P., Mostoslavsky, G., Franco, S., Murphy, M.M., et al. (2006). Genomic instability and aging-like phenotype in the absence of mammalian SIRT6. Cell *124*, 315–329.

Nagy, L., Kao, H.Y., Chakravarti, D., Lin, R.J., Hassig, C.A., Ayer, D.E., Schreiber, S.L., and Evans, R.M. (1997). Nuclear receptor repression mediated by a complex containing SMRT, mSin3A, and histone deacetylase. Cell *89*, 373–380.

Nan, X., Ng, H.H., Johnson, C.A., Laherty, C.D., Turner, B.M., Eisenman, R.N., and Bird, A. (1998). Transcriptional repression by the methyl-CpG-binding protein MeCP2 involves a histone deacetylase complex. Nature *393*, 386–389.

Narita, T., Yamaguchi, Y., Yano, K., Sugimoto, S., Chanarat, S., Wada, T., Kim, D.K., Hasegawa, J., Omori, M., Inukai, N., et al. (2003). Human transcription elongation factor NELF: identification of novel subunits and reconstitution of the functionally active complex. Mol. Cell. Biol. *23*, 1863–1873.

Nechaev, S., Fargo, D.C., dos Santos, G., Liu, L., Gao, Y., and Adelman, K. (2010). Global analysis of short RNAs reveals widespread promoter-proximal stalling and arrest of Pol II in Drosophila. Science *327*, 335–338.

Pavri, R., Zhu, B., Li, G., Trojer, P., Mandal, S., Shilatifard, A., and Reinberg, D. (2006). Histone H2B monoubiquitination functions cooperatively with FACT to regulate elongation by RNA polymerase II. Cell *125*, 703–717.

Petesch, S.J., and Lis, J.T. (2012). Overcoming the nucleosome barrier during transcript elongation. Trends Genet. *28*, 285–294.

Ping, Y.H., and Rana, T.M. (2001). DSIF and NELF interact with RNA polymerase II elongation complex and HIV-1 Tat stimulates P-TEFb-mediated phosphorylation of RNA polymerase II and DSIF during transcription elongation. J. Biol. Chem. *276*, 12951–12958.

Pokholok, D.K., Harbison, C.T., Levine, S., Cole, M., Hannett, N.M., Lee, T.I., Bell, G.W., Walker, K., Rolfe, P.A., Herbolsheimer, E., et al. (2005). Genome-wide map of nucleosome acetylation and methylation in yeast. Cell *122*, 517–527.

Ponnusamy, M.P., Deb, S., Dey, P., Chakraborty, S., Rachagani, S., Senapati, S., and Batra, S.K. (2009). RNA polymerase II associated factor 1/PD2 maintains self-renewal by its interaction with Oct3/4 in mouse embryonic stem cells. Stem Cells *27*, 3001–3011.

Rahl, P.B., and Young, R.A. (2014). MYC and transcription elongation. Cold Spring Harb. Perspect. Med. *4*, a020990.

Rahl, P.B., Lin, C.Y., Seila, A.C., Flynn, R.A., McCuine, S., Burge, C.B., Sharp, P.A., and Young, R.A. (2010). c-Myc regulates transcriptional pause release. Cell *141*, 432–445.

Rahman, S., Sowa, M.E., Ottinger, M., Smith, J.A., Shi, Y., Harper, J.W., and Howley, P.M. (2011). The Brd4 extraterminal domain confers transcription activation independent of pTEFb by recruiting multiple proteins, including NSD3. Mol. Cell. Biol. *31*, 2641–2652.

Ram, O., Goren, A., Amit, I., Shoresh, N., Yosef, N., Ernst, J., Kellis, M., Gymrek, M., Issner, R., Coyne, M., et al. (2011). Cell *147*, 1628–1639.

Ramirez, F., Ryan, D.P., Gruning, B., Bhardwaj, V., Kilpert, F., Richter, A.S., Heyne, S., Tundra, F., and Manke, T. (2016). deepTools2: a next generation web server for deep-sequencing data analysis. Nucleic Acids Res. *44*, W160–W165.

Rigbolt, K.T., Prokhorova, T.A., Akimov, V., Henningsen, J., Johansen, P.T., Kratchmarova, I., Kassem, M., Mann, M., Olsen, J.V., and Blagoev, B. (2011). System-wide temporal characterization of the proteome and phosphoproteome of human embryonic stem cell differentiation. Sci. Signal. *4*, rs3.

Robinson, J.T., Thorvaldsdóttir, H., Winckler, W., Guttman, M., Lander, E.S., Getz, G., and Mesirov, J.P. (2011). Integrative genomics viewer. Nat. Biotechnol. *29*, 24–26.

Ross-Innes, C.S., Stark, R., Teschendorff, A.E., Holmes, K.A., Ali, H.R., Dunning, M.J., Brown, G.D., Gojis, O., Ellis, I.O., Green, A.R., et al. (2012). Differential oestrogen receptor binding is associated with clinical outcome in breast cancer. Nature *481*, 389–393.

Samarakkody, A., Abbas, A., Scheidegger, A., Warns, J., Nnoli, O., Jokinen, B., Zarns, K., Kubat, B., Dhasarathy, A., and Nechaev, S. (2015). RNA polymerase II pausing can be retained or acquired during activation of genes involved in the epithelial to mesenchymal transition. Nucleic Acids Res. *43*, 3938–3949.

Schneider, D.A., French, S.L., Osheim, Y.N., Bailey, A.O., Vu, L., Dodd, J., Yates, J.R., Beyer, A.L., and Nomura, M. (2006). RNA polymerase II elongation factors Spt4p and Spt5p play roles in transcription elongation by RNA polymerase I and rRNA processing. Proc. Natl. Acad. Sci. USA *103*, 12707–12712.

Sebastián, C., Satterstrom, F.K., Haigis, M.C., and Mostoslavsky, R. (2012a). From sirtuin biology to human diseases: an update. J. Biol. Chem. *287*, 42444–42452.

Sebastián, C., Zwaans, B.M., Silberman, D.M., Gymrek, M., Goren, A., Zhong, L., Ram, O., Truelove, J., Guimaraes, A.R., Toiber, D., et al. (2012b). The histone deacetylase SIRT6 is a tumor suppressor that controls cancer metabolism. Cell *151*, 1185–1199.

Shen, C., Ipsaro, J.J., Shi, J., Milazzo, J.P., Wang, E., Roe, J.S., Suzuki, Y., Pappin, D.J., Joshua-Tor, L., and Vakoc, C.R. (2015). NSD3-Short Is an Adaptor Protein that Couples BRD4 to the CHD8 Chromatin Remodeler. Mol. Cell *60*, 847–859.

Silberman, D.M., Ross, K., Sande, P.H., Kubota, S., Ramaswamy, S., Apte, R.S., and Mostoslavsky, R. (2014). SIRT6 is required for normal retinal function. PLoS ONE *9*, e98831.

Skene, P.J., Henikoff, J.G., and Henikoff, S. (2018). Targeted in situ genome-wide profiling with high efficiency for low cell numbers. Nat. Protoc. *13*, 1006–1019.

Stasevich, T.J., Hayashi-Takanaka, Y., Sato, Y., Maehara, K., Ohkawa, Y., Sakata-Sogawa, K., Tokunaga, M., Nagase, T., Nozaki, N., McNally, J.G., and Kimura, H. (2014). Regulation of RNA polymerase II activation by histone acetylation in single living cells. Nature *516*, 272–275.

Strikoudis, A., Lazaris, C., Trimarchi, T., Galvao Neto, A.L., Yang, Y., Ntziachristos, P., Rothbart, S., Buckley, S., Dolgalev, I., Stadtfeld, M., et al. (2016). Regulation of transcriptional elongation in pluripotency and cell differentiation by the PHD-finger protein Phf5a. Nat. Cell Biol. *18*, 1127–1138.

Tasselli, L., Xi, Y., Zheng, W., Tennen, R.I., Odrowaz, Z., Simeoni, F., Li, W., and Chua, K.F. (2016). SIRT6 deacetylates H3K18ac at pericentric chromatin to prevent mitotic errors and cellular senescence. Nat. Struct. Mol. Biol. *23*, 434–440.

Thomas, P.D., Kejariwal, A., Campbell, M.J., Mi, H., Diemer, K., Guo, N., Ladunga, I., Ulitsky-Lazareva, B., Muruganujan, A., Rabkin, S., et al. (2003). PANTHER: a browsable database of gene products organized by biological function, using curated protein family and subfamily classification. Nucleic Acids Res. *31*, 334–341.

Thorvaldsdóttir, H., Robinson, J.T., and Mesirov, J.P. (2013). Integrative Genomics Viewer (IGV): high-performance genomics data visualization and exploration. Brief. Bioinform. *14*, 178–192.

Toiber, D., Erdel, F., Bouazoune, K., Silberman, D.M., Zhong, L., Mulligan, P., Sebastian, C., Cosentino, C., Martinez-Pastor, B., Giacosa, S., et al. (2013). SIRT6 recruits SNF2H to DNA break sites, preventing genomic instability through chromatin remodeling. Mol. Cell *51*, 454–468.

Tong, J.K., Hassig, C.A., Schnitzler, G.R., Kingston, R.E., and Schreiber, S.L. (1998). Chromatin deacetylation by an ATP-dependent nucleosome remodelling complex. Nature *395*, 917–921.

Van Oss, S.B., Cucinotta, C.E., and Arndt, K.M. (2017). Emerging Insights into the Roles of the Paf1 Complex in Gene Regulation. Trends Biochem. Sci. *42*, 788–798.

Vos, S.M., Farnung, L., Boehning, M., Wigge, C., Linden, A., Urlaub, H., and Cramer, P. (2018a). Structure of activated transcription complex Pol II-DSIF-PAF-SPT6. Nature *560*, 607–612.

Vos, S.M., Farnung, L., Urlaub, H., and Cramer, P. (2018b). Structure of paused transcription complex Pol II-DSIF-NELF. Nature *560*, 601–606.

Wada, T., Takagi, T., Yamaguchi, Y., Ferdous, A., Imai, T., Hirose, S., Sugimoto, S., Yano, K., Hartzog, G.A., Winston, F., et al. (1998). DSIF, a novel transcription elongation factor that regulates RNA polymerase II processivity, is composed of human Spt4 and Spt5 homologs. Genes Dev. *12*, 343–356.

Wang, G., Balamotis, M.A., Stevens, J.L., Yamaguchi, Y., Handa, H., and Berk, A.J. (2005). Mediator requirement for both recruitment and postrecruitment steps in transcription initiation. Mol. Cell *17*, 683–694.

Wei, P., Garber, M.E., Fang, S.M., Fischer, W.H., and Jones, K.A. (1998). A novel CDK9-associated C-type cyclin interacts directly with HIV-1 Tat and mediates its high-affinity, loop-specific binding to TAR RNA. Cell *92*, 451–462.

Winter, G.E., Mayer, A., Buckley, D.L., Erb, M.A., Roderick, J.E., Vittori, S., Reyes, J.M., di Iulio, J., Souza, A., Ott, C.J., et al. (2017). BET Bromodomain Proteins Function as Master Transcription Elongation Factors Independent of CDK9 Recruitment. Mol. Cell *67*, 5–18.

Wong, M., Tee, A.E.L., Milazzo, G., Bell, J.L., Poulos, R.C., Atmadibrata, B., Sun, Y., Jing, D., Ho, N., Ling, D., et al. (2017). The Histone Methyltransferase DOT1L Promotes Neuroblastoma by Regulating Gene Transcription. Cancer Res. *77*, 2522–2533.

Xue, Y., Wong, J., Moreno, G.T., Young, M.K., Côté, J., and Wang, W. (1998). NURD, a novel complex with both ATP-dependent chromatin-remodeling and histone deacetylase activities. Mol. Cell *2*, 851–861.

Yamada, T., Yamaguchi, Y., Inukai, N., Okamoto, S., Mura, T., and Handa, H. (2006). P-TEFb-mediated phosphorylation of hSpt5 C-terminal repeats is critical for processive transcription elongation. Mol. Cell *21*, 227–237.

Yamaguchi, Y., Takagi, T., Wada, T., Yano, K., Furuya, A., Sugimoto, S., Hasegawa, J., and Handa, H. (1999). NELF, a multisubunit complex containing RD, cooperates with DSIF to repress RNA polymerase II elongation. Cell *97*, 41–51.

Yang, Z., Yik, J.H., Chen, R., He, N., Jang, M.K., Ozato, K., and Zhou, Q. (2005). Recruitment of P-TEFb for stimulation of transcriptional elongation by the bromodomain protein Brd4. Mol. Cell *19*, 535–545.

Yang, B., Zwaans, B.M., Eckersdorff, M., and Lombard, D.B. (2009). The sirtuin SIRT6 deacetylates H3 K56Ac in vivo to promote genomic stability. Cell Cycle *8*, 2662–2663.

Yu, M., Yang, W., Ni, T., Tang, Z., Nakadai, T., Zhu, J., and Roeder, R.G. (2015). RNA polymerase II-associated factor 1 regulates the release and phosphorylation of paused RNA polymerase II. Science *350*, 1383–1386.

Zhang, Y., Iratni, R., Erdjument-Bromage, H., Tempst, P., and Reinberg, D. (1997). Histone deacetylases and SAP18, a novel polypeptide, are components of a human Sin3 complex. Cell *89*, 357–364.

Zhang, Y., Liu, T., Meyer, C.A., Eeckhoute, J., Johnson, D.S., Bernstein, B.E., Nusbaum, C., Myers, R.M., Brown, M., Li, W., and Liu, X.S. (2008). Model-based analysis of ChIP-Seq (MACS). Genome Biol. *9*, R137.

Zhong, L., D'Urso, A., Toiber, D., Sebastian, C., Henry, R.E., Vadysirisack, D.D., Guimaraes, A., Marinelli, B., Wikstrom, J.D., Nir, T., et al. (2010). The histone deacetylase Sirt6 regulates glucose homeostasis via Hif1alpha. Cell *140*, 280–293.

STAR★METHODS

KEY RESOURCES TABLE

REAGENT or RESOURCE	SOURCE	IDENTIFIER
Antibodies		
Rabbit anti-SIRT6	Cell Signaling Tech	Cat#12486S; RRID: AB_2636969
Rabbit anti-H3K56ac	Abcam	Cat#ab76307; RRID: AB_1523762
Rabbit anti-H3K9ac	Abcam	Cat#ab1791; RRID: AB_302613
Mouse anti-Pol II (Rpb1)	Cell Signaling Tech	Cat#2629; RRID: AB_2167468
Rabbit anti NELF-E	Abcam	Cat# ab170104
Rabbit anti-AFF4	Lin et al., 2010	N/A
Rabbit anti-ELL2	Lin et al., 2010	N/A
Chemicals, Peptides, and Recombinant Proteins		
5,5,6 5,6 Dichlorobenzimidazole 1-β-D-ribofuranoside	Sigma-Aldrich	D1916
GST-CTD Pol II	Abcam	ab81888
Protein A-MNase	Skene et al., 2018	N/A
Biotin-11-CTP	PerkinElmer	NEL542001EA
Biotin-11-UTP	PerkinElmer	NEL543001EA
Biotin-11-ATP	PerkinElmer	NEL544001EA
Biotin-11-GTP	PerkinElmer	NEL545001EA
Critical Commercial Assays		
RNA TriPure Isolation Reagent	Roche	Cat #11 667 157 001
QuantiTect Reverse Transcription Kit	QIAGEN	Cat #205310
SYBR green master Mix	Roche	Cat #04 707 516 001
Deposited Data		
Raw and analyzed data	This paper	Database GEO: GSE130689
		Database GEO: GSE130690
		Database GEO: GSE130691
		Database GEO: GSE130692
Experimental Models: Cell Lines		
SIRT6 KO Embryonic Stem Cells (ES) cells	Mostoslavsky et al., 2006	N/A
Oligonucleotides		
Primers for Pro-seq, see STAR Methods	This paper	N/A
Primer: GFP/YFP/CFP Forward: GCACGACTTCTTCA AGTCCGCCATGCC	This paper	N/A
Software and Algorithms		
tophat2 version 2.0.10	Kim et al., 2013	http://ccb.jhu.edu/software/tophat
HTseq version 0.6.1	Anders et al., 2015	https://htseq.readthedocs.io/en/release_0.11.1/
DESeq2	Love et al., 2014	https://bioconductor.org/packages/release/bioc/html/DESeq2.html
bwa version 0.7.13	Li and Durbin, 2010	http://bio-bwa.sourceforge.net
Diffbind	Ross-Innes et al., 2012	https://bioconductor.org/packages/release/bioc/html/DiffBind.html
MACS2 version 2.1	Zhang et al., 2008	https://github.com/taoliu/MACS
Picard tools	N/A	http://picard.sourceforge.net
Prism v8.1.2	N/A	https://www.graphpad.com/scientific-software/prism/
bowtie v1.2.2	N/A	http://bowtie-bio.sourceforge.net/index.shtml
cutadapt v1.14	N/A	https://cutadapt.readthedocs.io/en/stable/

LEAD CONTACT AND MATERIALS AVAILABILITY

Further information and requests for resources and reagents should be directed to and will be fulfilled by the Lead Contact, Raul Mostoslavsky (rmostoslavsky@mgh.harvard.edu).

EXPERIMENTAL MODEL AND SUBJECT DETAILS

Cell lines

SIRT6 KO and WT ESCs in 129 strain genetic background (Mostoslavsky et al., 2006) were maintained on γ-irradiated mouse embryonic fibroblasts (MEFs) in knockout DMEM medium (GIBCO) containing 15% ES-qualified FBS, 0.1 mM each of non-essential amino acids, 2 mM L-glutamine, 0.1 mM β-mercaptoethanol, 50 units ml^{-1} penicillin/streptomycin (Invitrogen) and supplemented with leukemia inhibiting factor (LIF). For all experiments described, cells were trypsinized and plated for 30 min on standard tissue culture dishes to remove feeder cells before floating ESCs were collected and re-plated on gelatin-coated dishes. For siRNA-mediated knockdowns of BRD4, MYC and/or PAF1 we transfected synthetic siRNA oligos using Lipofectamine 2000, according to the manufacturers protocol. The siRNA for BRD4 targets all mouse BRD4 isoforms (siGENOME SMARTpool from Dharmacon). Hence, BRD4 protein levels were almost undetectable by western blot analysis. The expression of MYC and PAF1 was also knocked down using siGENOME SMARTpool siRNA oligos from Dharmacon. For MYC knockdown we used two siRNA systems, the oligo duplex (27-mers) from OriGene and siGENOME SMARTpool from Dharmacon. For glucose deprivation experiments, ESCs were cultured with glucose-free DMEM with 15% FBS 0.1 mM each of non-essential amino acids, 2 mM L-glutamine, 0.1 mM β-mercaptoethanol, 50 units ml^{-1} penicillin/streptomycin (Invitrogen) and supplemented with LIF for 2 days before harvesting cells for biochemical assays.

METHOD DETAILS

Antibodies

The antibodies used for western blot analysis are: anti-SIRT6 (Abcam, ab62739), anti-NELF-E (Santa Cruz, sc32912), anti-Pol II (Cell Signaling Tech., 2629), anti-Pol II S5P (Abcam, ab5131), anti-Pol II S2P (Millipore, 04-1571), anti-MYC (Abcam, ab32072), anti-BRD4 (Bethyl, 0301-985A50), anti-MED23 (BD PharMingen, 550429), anti-PAF1(D9G9X) (Cell Signaling Tech., 12883S), anti-LEO1 (Bethyl, A300-175A), anti-CDK9 (Santa Cruz, sc-8338), anti-SPT5 (Bethyl., A300-868A), anti-PDK1 (Cell Signaling Tech., 3062S), anti-LDHA (Cell Signaling Tech., 2012S), anti-phospho-pan antibody (Invitrogen, 61-8300), anti-Tubulin (Abcam, ab6160), Rabbit plyclonal anti-AFF4 and anti-ELL2 antibodies (provided by Ali Shilatifard), anti-H3K9ac (Millipore, 07-352), anti-H3K56ac (Abcam, ab76307), anti-H3 (Abcam, ab1791) and anti-actin (Sigma-Aldrich, A2066). Protein-protein immunoprecipitations were performed as previously described (Lee et al., 2001). Antibodies targeting the super elongation factors AFF4 and ELL2 were provided by Ali Shilatifard.

The antibodies used for ChIP-RTqPCR, ChIP-seq and CUT&RUN analysis are: anti-MYC (Abcam, ab32072), anti-AFF4 and anti-ELL2 antibodies (provided by Ali Shilatifard), anti-Pol II (Cell Signaling Tech., 2629), anti-SIRT6 (Cell Signaling Tech., 12486S), anti-H3K9ac (Millipore 07-352), anti-H3K56ac (Abcam, ab76307), anti-H3K79me2 (Cell Signaling Tech., 5472), anti-H3K36me3 (Cell Signaling Tech., 4909), anti-LEO1 (Bethyl, A300-175A) and anti-NELF-E (Abcam, ab170104).

Immunoblotting

Immunoblots were developed with HRP conjugated goat anti-rabbit (Sigma-Aldrich, AQ132P), goat anti-mouse (Sigma-Aldrich, A3682) or goat anti-rat (Santa Cruz Biotech., sc-2006) secondary antibodies and ECL Plus (GE healthcare Lifescience, RPN2133).

Chromatin extraction and western blot analysis

For chromatin extractions, cell pellets were resuspended in lysis buffer (10mM HEPES pH 7.4, 10 mM KCl, 0.05% NP-40) supplemented with a protease inhibitor cocktail (Complete EDTA-free, Roche Applied Science), 5 μM TSA, 5mM sodium butyrate, 1mM DTT, 1mM PMSF, 50mM NaF, 0.2mM sodium orthovanadate and phosphatase inhibitors (Phosphatase Inhibitor Cocktail Sets I and II, Calbiochem) and incubated on ice for 20 min. The lysate was then centrifuged at 14,000 rpm for 10 min at 4°C. The supernatant was removed (cytosolic fraction) and the pellet (nuclei) was acid-extracted using 0.2N HCl and incubated on ice for 20 min. The lysate was then centrifuged at 14,000 rpm for 10 min at 4°C. The supernatant (contains acid soluble proteins) was neutralized using 1M Tris-HCl pH 8. Protein concentration was measured by Biorad Protein Assay. Western blot analyses were performed as previously described (Zhong et al., 2010). Briefly, 10 ug of protein was loaded on a 10%–20% gradient polyacrylamide gel with SDS (Biorad) and electroblotted onto polyvinylidene difluoride membranes (PVDF) (Millipore). Membranes were blocked in TBS with 5% non-fat milk and 0.1% Tween and probed with antibodies. Bound proteins were detected with horseradish-peroxidase-conjugated secondary antibodies (Vector Biolaboratories) and SuperSignal West Pico Luminol/Enhancer Solution (Thermo Scientific).

CDK9 Kinase Assay

Cells were collected in cold PBS and lysed in cold EBC buffer (50 mM Tris-HCl pH 8.0, NaCl 120 mM, 0.5% NP-40, 5 mM DTT). After pre-clearing with protein-A beads for 2 hours at 4°C, the lysates were incubated with either 3 ug CDK9 antibody (Santa Cruz

sc-8338x) or equal amount of IgG antibody control (Sigma-Aldrich, 12-370) under constant rotation at 4°C overnight. The beads were then washed 3 times with EBC + 0.05% SDS, then once with TKB/Mg buffer (50 mM HEPES pH 7.5, 10 mM MgCl2, 5 mM DTT). The beads were resuspend in 25 ul of TKB/Mg buffer plus 2.5 mM MnCl2, 5 uM ATP, 200ng GST-CTD (Abcam ab81888), and 5 uCi γ-^{32}P-ATP and incubated at room temperature for 40 minutes with or without 50 uM of the CDK9 inhibitor DRB (5,6-Dichlorobenzimidazole 1-β-D-ribofuranoside) (Sigma-Aldrich, D1916). The reactions were stopped by adding 18 ul of 4x SDS loading buffer and boil the sample 10 minutes at 95°C. Samples were loaded in a polyacrylamide gel, which was then fixed with 40% methanol + 10% acetic acid for 30 min. Gels were washed three times for 5 min with Milli-Q H_2O and stained with BioRad Coomassie (161-0786) for 1 hour at room temperature. Additional washes with ddH_2O were done to clear the background. Finally, the gel was dried under a vacuum system, exposed and developed.

Protein-protein Immunoprecipitations

Protein-protein immunoprecipitations were performed as previously described (Lee et al., 2001). Briefly, whole cell lysates or chromatin fractions were subjected to immunoprecipitation using magnetic Dynabeads Protein-A (Invitrogen, 10006D) or Protein-G (Invitrogen, 10007D) immunoprecipitation kits. Prior immunoprecipitation, magnetic beads were conjugated with specific primary antibodies (see list of antibodies above). Samples were incubated at 4°C with constant rotation overnight in IP buffer (20 mM HEPES pH 7.5, 1 mM EDTA, 5 mM NaF, 1 mM DTT, 0.05% Triton X-100, 5% glycerol, 0.25 mM PMSF plus protease inhibitors cocktail tablets [Sigma-Aldrich, 4693116001]). Magnetic dynabeads containing immunoprecipitated samples were then washed twice with IP buffer and 3 times with washing buffer supplied in the Dynabead kit.

RNA extraction and quantitative PCR with reverse transcription

Total RNA was extracted with the TriPure Isolation Reagent (Roche) as described by the manufacturer. For cDNA synthesis, 1 mg of total RNA was retro-transcribed by using the QuantiTect Reverse Transcription Kit (QIAGEN). Real-time PCR was performed using the SYBR green master mix (Roche), following the manufacturer's instructions, with the exception that the final volume was 12.5 mL of SYBR green reaction mix. Real-time monitoring of PCR amplification was performed using the LightCycler 480 detection system (Roche). Data were expressed as relative mRNA levels normalized to the β-actin expression level in each sample. The primer sequences can be obtained on request. For RNA-Seq, total RNA purified with TriPure was cleaned up with RNeasy kits from QIAGENe.

In vitro transcription elongation assay

The *in vitro* transcription elongation assay was performed and analyzed as described earlier (Kim et al., 2010). Briefly, after the second gel filtration, approximately 35 ng plasmid DNA-containing chromatin template was mixed with nuclear extract containing total 5 μg protein which were prepared from control or SIRT6 knockdown HeLa cells. The extracts were adjusted to TX-buffer condition prior to the addition. The reactions were 50ul in this step and incubated for 30 min at 30°C. The reactions were then added with nucleotides and RNasin in total 5 ul, and also adjusted to TX-buffer condition, which bring the final volume to 55ul, to allow the transcription elongation. At the indicated time point, the reactions were stopped and transcription products were resolved by acrylamide gel electrophoresis and visualized by X-ray film.

Permanganate footprinting

Ligation Mediated PCR (LM-PCR) based permanganate footprinting was done as described (Samarakkody et al., 2015). In brief, cells were washed with 1xPBS and treated with 20mM $KMn0_4$ for 60 s on ice. Reactions were quenched with Stop buffer (1% SDS, 10mM Tris HCl pH 8.0, 20mM EDTA, 0.5 M 2-mercaptoethanol) and, after treatment with RNase cocktail (Ambion), Proteinase K and extraction with phenol-chloroform, DNA was ethanol-precipitated and resuspended in water at approximately 100 ng/μl. Up to 5 μg of DNA was treated with 10% (v/v) piperidine in the final volume 100 μl, for 10 minutes at 90°C, after which DNA was extracted with chloroform twice, ethanol precipitated in the presence of 10 μg GlycoBlue carrier, and resuspended in water at approximately 50 ng/μl. Previously purified genomic DNA (naked DNA) was treated with permanganate and piperidine as above to establish background DNA reactivity. Template for the A+G sequencing ladder was generated by treating purified DNA with formic acid (Maxam and Gilbert, 1977) followed by piperidine treatment as above. Approximately 200 ng of piperidine-treated DNA was taken for each Ligation-mediated (LM) PCR reaction. LM PCR began with primer extension with Primer A with Phusion DNA polymerase followed by the addition of universal double-stranded linker (Samarakkody et al., 2015) and ligation with T4 DNA ligase. After ethanol precipitation, the ligated template was used for 22 cycles of PCR with gene-specific Primer B and Linker-specific primers, after which 5′-32P-labeled primer was added and PCR continued for another 2 cycles. After phenol extraction and ethanol precipitation, DNA was resuspended in 5 μl of 7M urea-1xTBE loading buffer and resolved on denaturing polyacrylamide sequencing gel followed by radioautography. Footprints were quantified using ImageJ by subtracting the signal from naked DNA from reactivity of cells within the pausing region. Primer sequences can be provided upon request.

Chromatin immunoprecipitation assays

Chromatin immunoprecipitation (ChIP) assays were performed as previously described (Gomes et al., 2006). Briefly, ESCs were crosslinked with 1% formaldehyde/PBS for 15 min at room temperature. Crosslinking was quenched by addition of 0.125 M glycine.

ESCs were washes twice with ice-cold PBS, and then collected in RIPA buffer as described previously. Samples were then sonicated to generate DNA fragments of approximately 0.5 kb. Approximately, 1 μg of pre-cleared protein extract was used for immunoprecipitation with the following specific antibodies: anti-Pol II (Cell Signaling Tech., 2629), anti-SIRT6 (Cell Signaling Tech., 12486S), anti-NELF-E (Abcam), anti-MYC (Abcam, ab32072), anti- LEO1 (Bethyl, A300-175A). Antibodies targeting the super elongation factors AFF4 and ELL2 were provided by Ali Shilatifard. Immunoprecipitation was performed for approximately 12 hours at 4°C using protein A/G plus agarose beads (Santa Cruz, sc2003). Bead-containing samples were then washed as previously described (Gomes et al., 2006). Immunocomplexes were eluted by incubation at 65°C for 10 min in the presence of 1% SDS, and crosslinking was reversed by 6 h incubation at 65°C in the presence of 200 mM NaCl. DNA was purified by the QIAquick spin kit (QIAGEN) and further assessed by qPCR using the LightCycler 480 system from Roche. Data were normalized to input and expressed relative to the nonspecific IgG or IgM ChIP controls. Primer sequences can be obtained on request.

ChIP-seq

Chromatin samples were prepared as previously described (Mishra et al., 2018). In brief, ESCs grown on 15 cm dish were crosslinked with 1% formaldehyde for 10 min at 37°C. Crosslinking was quenched with 0.125M glycine for 5 min at 37°C. Collected cell pellets from each 15 cm dish were resuspended in 2.5 mL lysis buffer supplemented with protease inhibitors (5 mM PIPES pH8, 85 mM KCL, 0.5% NP40) and incubated 5 min at 4°C. Chromatin was obtained by centrifugation at 800 rpm for 5 min at 4°C, where nuclear fraction from approximately 10 to 12 million cells were resuspended in 300 μL of nuclear lysis buffer (50 mM Tris-HCL pH8, 10 mM EDTA pH8, 0.2% SDS). Chromatin was then sonicated at 70% amplitude 15 s ON and 45 s OFF for 45 min. About 5 μL of sonicated chromatin was reverse-crosslinked with 1 μL of proteinase K in elution buffer (50 mM $NaHCO_3$, 140 mM NaCl, 1% SDS) at 65°C overnight. After RNase treatment, DNA was isolated by phenol chloroform extraction and analyzed on 1% agarose gel electrophoresis. Only samples with smear below 300 bp were used for ChIP-seq analysis. Approximately 10 to 30 μg of pre-cleared chromatin was used per each immunoprecipitation with magnetic beads conjugated with ~2 μg of antibody in IP buffer (16.7 mM Tris HCL pH8, 1.2 mM EDTA pH8, 167 mM NaCl, 0.01% SDS, 1.1% Triton x-100) at 4°C overnight. The immunoprecipitated DNA was washed twice with IP buffer, once with TSE buffer (20 mM Tris HCL pH8, 2 mM EDTA pH8, 500 mM NaCl, 1% Triton x-100, 0.1% SDS), once with LiCl buffer (100 mM Tris HCL pH8, 500 mM LiCl, 1% deoxycholic acid, 1% NP40) and twice with TE-buffer (10 mM Tris-HCL pH8, 1 mM EDTA pH8) before elution by incubation in elution buffer (50 mM $NaHCO_3$, 140 mM NaCl, 1% SDS) supplemented with 10 μg of proteinase K at 55°C for 1 hour. The samples were removed from the magnetic beads and reverse-crosslinked at 65°C for 4 hr. Immunoprecipitated DNA was purified using PCR purification columns from QIAGEN. Construction of the DNA libraries for DIP sequencing were performed with Illumina reagents and sequencer equipment.

Chromatin immunoprecipitations were performed with the following antibodies: from Cell Signaling Technology we used anti-Pol II(Rpb1 CTD, 4H8) (Cat# 2629), anti-SIRT6(D8D12) (Cat# 12486S), anti-H3K79me2(D15E8) (Cat# 5472), anti-H3K36me3(D5A7) (Cat# 4909); Anti-H3K9ac (Millipore 07-352), anti-H3K56ac (abcam ab76307), and anti-LEO1 (Bethyl A300-175A).

ChIP-seq Heatmap Creation

Reads from RNA Pol II, SIRT6, and HDACI ChIP-seq for both WT and SIRT6 KO ESCs were aligned to mouse genome mm9 using bwa and duplicate reads were marked with Picard tools (http://picard.sourceforge.net). The heatmaps of Figure 2A were produced by calculating the mean coverage values of 100bp windows in the ± 3kb region centered on the TSS for all genes using the ChIP-seq data for SIRT6 and Pol II in ESC cells. The heatmaps represent the mean enrichment by bin after correcting for the direction of the DNA strand. For the heatmap after filtering out genes with insufficient signal, coverage values for the genes z-score normalized and then ordered by hierarchical clustering using Euclidean distance and Ward method of the R heatmap.2 function. The list includes genes that passed the cutoffs for at least one of Pol II, and SIRT6, and only the top 400 genes for each sample are displayed. To assess the enrichment of ChIP-seq signal across gene body regions (Figure 2E), we calculated the ratio of ChIP to input sequencing tag number in the region of the gene body excluding the immediate 3 Kb proximity of TSS. These enrichment values for the gene set of interest were compared between Sirt6 KO and wild-type using t test.

CUT&RUN

These experiments were performed as described by Skene and Henikoff (Skene et al., 2018) with modifications. Briefly, mouse ESCs (~1 million) were fixed with 1% paraformaldehyde (PFA) and quenched with 125 mM glycine. After centrifugation at ~400xg, cell pellets were washed three times with PBS and twice with HEPES buffer (20 mM HEPES pH 7.5, 150 mM NaCl, 0.5% BSA, 0.1% Tween 20). Activated concanavalin A-coated magnetic beads (Bangs Laboratories) were added to capture the cells, which were incubated at 4°C overnight with antibodies targeting H3K27me3 (cell Signaling Cat# 9733), H3K9ac (Millipore Cat# 07-352), NELF-E (Abcam Cat# ab170104), IgG control (Antibody-online Cat# ABIN101961). IgG and H3K27me3 antibodies served as negative and positive controls, respectively. Immunoprecipitated samples were supplemented with protein A-MNase (700 ng/ml) and incubated for 1 hour at 4°C and placed on ice. Protein A-MNase was activated by incubation with 2 mM CaCl2 on ice for 30 min. This reaction was terminated with stop buffer (340 mM NaCl, 20 mM EDTA, 4 mM EGTA, 0.1% Tween 20, 50 ug/ml RNaseA, 50 ug/ml glycogene, 0.05 pg/ml heterologous yeast spike-in DNA). CUT&RUN fragments were released by incubation at 37°C

for 10 min followed by centrifugation. Immunoprecipitated DNA was purified by QIAquick Gel extraction kit (QIAGEN Cat# 28706). Library preparations were done based on Skene and Henikoff method (Skene et al., 2018) followed by Tapestation analysis to assess the quality of DNA libraries.

PRO-seq library preparation and data analysis

Wild-type mouse ESCs of (WT), or SIRT6-KO (KO) genotypes, or WT cells that were glucose-starved (No Glucose) for 48hr. were permeabilized at 4°C or on ice unless otherwise specified. Briefly, cells were washed once in ice-cold 1x PBS and resuspended in Buffer W (10 mM Tris-HCl pH 8.0, 10% glycerol, 250 mM sucrose, 10 mM KCl, 5 mM $MgCl_2$, 0.5 mM DTT, protease inhibitors cocktail (Roche), and 4 u/mL RNase inhibitor (SUPERaseIN, Ambion)) at the cell density of 2×10^7 cells/mL. 9x volume of Buffer P (10 mM Tris-HCl pH 8.0, 10% glycerol, 250 mM sucrose, 10 mM KCl, 5 mM $MgCl_2$, 0.5 mM DTT, 0.1% Igepal, protease inhibitors cocktail (Roche), 4 u/mL RNase inhibitor (SUPERaseIN, Ambion)) was then immediately added. Cells were gently resuspended and incubated for up to 2 min on ice. Cells were then recovered by centrifugation (800 x *g* for 4 min) and washed in Buffer F (50 mM Tris-HCl pH 8.0, 40% glycerol, 5 mM $MgCl_2$, 0.5 mM DTT, 4 u/mL RNase inhibitor [SUPERaseIN, Ambion]). Washed permeabilized cells were finally resuspended in Buffer F at a density of 1×10^6 cells/30 μL and immediately frozen in liquid nitrogen. Permeabilized cells were stored in −80°C until usage.

PRO-seq run-on reactions were carried out as follows: 1×10^6 permeabilized cells spiked with 5×10^4 permeabilized *Drosophila* S2 cells were added to the same volume of 2x Nuclear Run-On reaction mixture (10 mM Tris-HCl pH 8.0, 300 mM KCl, 1% Sarkosyl, 5 mM $MgCl_2$, 1 mM DTT, 200 μM biotin-11-A/C/G/UTP (Perkin-Elmer), 0.8 u/μL SUPERaseIN inhibitor (Ambion)) and incubated for 5 min at 30°C. Nascent RNA was extracted using a Total RNA Purification Kit following the manufacturer's instructions (Norgen Biotek Corp.). Extracted nascent RNA was fragmented by base hydrolysis in 0.25 N NaOH on ice for 10 min and neutralized by adding 1x volume of 1 M Tris-HCl pH 6.8. Fragmented nascent RNA was bound to 30 μL of Streptavidin M-280 magnetic beads (Thermo Fisher Scientific) in Binding Buffer (300 mM NaCl, 10 mM Tris-HCl pH 7.4, 0.1% Triton X-100). The beads were washed twice in High salt buffer (2 M NaCl, 50 mM Tris- HCl pH 7.4, 0.5% Triton X-100), twice in Binding buffer, and twice in Low salt buffer (5 mM Tris-HCl pH 7.4, 0.1% Triton X-100). Bound RNA was extracted from the beads using Trizol (Invitrogen) followed by ethanol precipitation.

For the first ligation reaction, fragmented nascent RNA was dissolved in H_2O and incubated with 10 pmol of reverse 3′ RNA adaptor (5′p-rNrNrNrNrNrGrArUrCrGrUrCrGrGrArCrUrGrUrArGrArArCrUrCrUrGrArArC-/3′InvdT/) and T4 RNA ligase I (NEB) under manufacturer's conditions for 2 h at 20°C. Ligated RNA was enriched with biotin-labeled products by another round of Streptavidin bead binding and washing (two washes each of High, Binding and Low salt buffers and one wash of 1x Thermo Pol Buffer (NEB)). To decap 5′ ends, the RNA products were treated with RNA 5′ Pyrophosphohydrolase (RppH, NEB) at 37°C for 30 min followed by one wash of High, Low and T4 PNK Buffer. To repair 5′ ends, the RNA products were treated with Polynucleotide Kinase (PNK, NEB) at 37°C for 30 min.

5′ repaired RNA was ligated to reverse 5′ RNA adaptor (5′-rCrCrUrUrGrGrCrArCrCrCrGrArGrArArUrUrCrCrA-3′) with T4 RNA ligase I (NEB) under manufacturer's conditions for 2 h at 20°C. Adaptor ligated nascent RNA was enriched with biotin-labeled products by another round of Streptavidin bead binding and washing (two washes each of High, Binding and Low salt buffers and one wash of 1x SuperScript IV Buffer (Thermo Fisher Scientific)), and reverse transcribed using 25 pmol RT primer (5′- AATGATACGGCGACCA CCGAGATCTACACGTTCAGAGTTCTACAGTCCGA-3′) for TRU-seq barcodes (RP1 primer, Illumina). A portion of the RT product was removed and used for trial amplifications to determine the optimal number of PCR cycles. For the final amplification, 12.5 pmol of RPI-index primers (for TRU-seq barcodes, Illumina) was added to the RT product with Phusion polymerase (NEB) under standard PCR conditions. Excess RT primer served as one primer of the pair used for the PCR. The product was amplified 12∼14 cycles and beads size selected (ProNex Purification System, Promega) before being sequenced in NextSeq 500 machines in a mid-output 150-bp cycle run.

PRO-seq libraries from 3 independent biological replicates (WT and KO) or 2 biological replicates (NG) were generated. Paired-end reads were trimmed to 40 nt, for adaptor sequence and low quality 3′ ends using cutadapt 1.14, discarding those containing reads shorter than 20 nt (-m 20 -q 10), and removing a single nucleotide from the 3′ end of all trimmed reads to allow successful alignment with Bowtie 1.2.2 (Langmead, Trapnell et al., Genome Biol. 10, R25, 2009). Remaining pairs were paired-end aligned to the dm3 genome index to determine spike-normalization ratios based on uniquely mapped reads. Mappable pairs were excluded from further analysis, and unmapped pairs were aligned to the mm9 genome assembly. Identical parameters were utilized in each alignment described above: up to 2 mismatches, maximum fragment length of 1000 nt, and uniquely mappable, and unmappable pairs routed to separate output files (-m1, -v2, -X1000,–un). Pairs mapping uniquely to mm9, representing biotin-labeled RNA 3′ ends, were separated, and strand-specific counts of the 3′ mapping positions determined at single nucleotide resolution, genome-wide, and expressed in bedGraph format with "plus" and "minus" strand labels swapped for each 3′ bedGraph, to correct for the "forward/reverse" nature of Illumina paired-end sequencing (Mahat et. al., 2016). Counts of pairs mapping uniquely to spike-in RNAs (*Drosophila* genome) were determined for each sample. Uniquely mappable reads were determined, and a normalization factor calculated. In this case, the spike in reads exhibited no systematic differences across samples, thus normalization based on sequencing depth was used for each bedGraph. PRO-seq size factors used were: for WT 1.70255924, 3.35361899, 1.04422773; KO: 2.19052323, 3.46076838, 1.00000000; and NG: 3.22211594, 3.16824971. To account for the different number of replicates used in No Glucose condition (N = 2) the WT and KO datasets (each N = 3) were downsampled by 2/3 to facilitate direct comparisons.

Combined bedGraphs were generated by summing counts per nucleotide of all replicates for each condition; and UCSC Genome Browser tracks displaying mean read coverage were generated from the combined replicates per condition, normalized as described above.

Sample	Total reads	Uniquely mapped reads (Percentage of total)	Agreement between replicates (Spearman's rho)
WT (Wild-type)	331,008,473	36.68%	> 0.97
KO (SIRT6-KO)	340,699,369	33.10%	> 0.97
NG (No-Glucose)	250,932,240	42.53%	0.99

Pausing Indices and composite analyses of PRO-seq signals

TSSs were designated as bound by Pol II if there were a total of 16 reads in WT bedGraphs (without normalization) in the region ± 150 bp from the annotated TSS. 12,941 of 17,032 TSSs (76.0%) were classified as Pol II-bound using this cutoff, of which 3,659 are upregulated genes in RNA-seq upon SIRT6-KO. Composite metagene distributions were generated by summing sequencing reads at each indicated position with respect to the TSS and dividing by the number of TSSs included within each group. These were plotted across a range of distances. Zoomed-in PRO-seq profiles (e.g., Figures 2G–2I) were smoothed by calculating a moving average across adjacent 5 bins.

QUANTIFICATION AND STATISTICAL ANALYSIS

Gene expression, transcription factor binding and *in vitro* transcription analysis

Standard 2-sample t test assuming equal variance was used to calculate gene expression levels, transcription factor binding and elongation products, from RT-qPCR, ChIP-qPCR and *in vitro* transcription elongation experiments, respectively. The "n" values represent a minimum of 3 biological replicas, and the error bars correspond to s.e.m. calculated using analysis of variance (ANOVA).

ChIP-seq analysis

Sequencing reads were aligned against the mm9 reference genome using BWA (Li and Durbin, 2010). Alignments were filtered for uniquely mapped reads and duplicates were removed. Input-normalized coverage tracks were generated using SPP; enrichment peaks were called using SPP as broad regions of enrichment with FDR cutoff of 0.01 (Kharchenko et al., 2008). Regions of differential tag enrichment were determined based on tag counts in all identified peak regions using Diffbind (Ross-Innes et al., 2012) with FDR cutoff 0.1. These regions of differential enrichment between SIRT6 KO and WT ESCs were then analyzed for the proximity (within 20 Kb) to the differentially expressed genes detected in RNA-seq analysis. Reads from H3K9Ac, H3K56Ac, H3K36me3, H3K79me2, Pol II, and LEO1 ChIP-seq for WT and SIRT6 KO ESCs, and H3 control for mouse ESCs were aligned to mouse genome mm9 using bwa and duplicate reads were marked with Picard tools (http://picard.sourceforge.net). Peaks were called using MACS2 version 2.1 with the False Discovery Rates (FDR) q = 0.01 with the '—broad' flag. A subset of called peaks were checked visually with the IGV browser. The Bioconductor package DiffBind was used to find differentially bound ChIP-seq peaks for all the histone marks and factors using H3 ChIP-seq as an input control. Differential binding statistics in DiffBind were calculated with DESeq2 with an FDR threshold of 0.1. Differentially bound peaks with FDR < 0.1 were assigned to genes if they fell within ± 20kb of the gene body using Bioconductor 'TxDb.Mmusculus.UCSC.mm9.knownGene' annotation. Gene Ontology (GO) categories were assigned to genes using the functional annotation table method in DAVID functional annotation tool version 6.8 (https://david.ncifcrf.gov). p values were obtained using standard 2-sample t test assuming equal variance. Pearson correlations between replicates were calculated by covering over 10Kb windows across the genome for all the different ChIP-seqs (see Figure S6).

Pausing Index calculated from Pol II ChIP-seq analysis

Reads from RNA Pol II ChIP-seq for WT and SIRT6 KO ESCs were aligned to mouse genome mm9 using bwa and duplicate reads were marked with Picard tools (http://picard.sourceforge.net). Pausing Indexes (PI) were calculated as the Pol II ChIP-seq density ratios between the promoter and the gene body regions in genes with significant Pol II signal in the promoter region (FDR < 1e-3 from SISSRs) generally following the methods used in Nechaev et al. (2010) and Henriques and Adelman (2013). The promoter was defined as the TSS ± 150bp while the gene body was defined as +250bp to +2250bp (or the gene end if the gene is less than 2250bp). Figure 2E shows the fraction of RNA Pol II bound genes with a PI greater than or equal to the value of the PI value on the x axis for WT and SIRT6 KO. Figure 2E shows average pausing for two replicates each of WT and SIRT6 KO ESC ChIP-seq data for RNA Pol II for genes that were upregulated in SIRT6 KO RNA-Seq samples with DESeq2 adjusted p value < 0.1 (4938 genes). There were 2459 unique genes that had greater than 2-fold decrease in pausing index for SIRT6 KO of the 4938 genes that were upregulated in SIRT6 KO ESCs (Tables S1 and S3).

RNA-Seq data analysis

Read counts were calculated per gene, in a strand-specific manner, based upon alignments to the UCSC mouse mm9 transcriptome using tophat2 version 2.0.10 and htseq version 0.6.1, and finally differentially expressed genes were found using the Bioconductor package DESeq2. Differentially expressed genes were defined using an adjusted p value threshold of < 0.1. Of 23,366 genes, 4938 were identified as differentially expressed upon SIRT6-KO in mESC cells. p values were obtained using standard 2-sample t test assuming equal variance.

CUT&RUN data analysis

CUT&RUN sequenced reads were aligned to mouse mm9 and yeast S288C reference genome using BWA. Mouse alignments were filtered for uniquely mapped reads and duplicates were removed, then mouse profiles were normalized to the number of aligned heterologous yeast spike-in genomic DNA reads. Metagene profiles were generated using deeptools (Ramirez et al., 2016).

Pausing Index calculated from PRO-seq analysis

Genomic statistical tests: Statistical significance for comparisons of promoter (±150 nt from TSS) and gene body (+250 to +1250 nt from TSS) between WT and KO or NG conditions was assessed by Mann-Whitney test. Statistical details and error bars are defined in each figure legend. Spearman correlations were calculated by using a ± 250bp window around promoters (N = 17032) of annotated genes for each of the replicates in WT, WT No Glucose or SIRT6-KO conditions (see Figure S7).

DATA AND CODE AVAILABILITY

GEO Accession numbers

All the raw datasets for the different sequencing experiments have been deposited in NCBI. The accession number for these different sequencing experiments are: GEO: GSE130689, GEO: GSE130690, GEO: GSE130691, and GEO: GSE130692.

Molecular Cell, Volume *75*

Supplemental Information

The Histone Deacetylase SIRT6 Restrains Transcription Elongation via Promoter-Proximal Pausing

Jean-Pierre Etchegaray, Lei Zhong, Catherine Li, Telmo Henriques, Eileen Ablondi, Tomoyoshi Nakadai, Capucine Van Rechem, Christina Ferrer, Kenneth N. Ross, Jee-Eun Choi, Ann Samarakkody, Fei Ji, Andrew Chang, Ruslan I. Sadreyev, Sridhar Ramaswamy, Sergei Nechaev, Johnathan R. Whetstine, Robert G. Roeder, Karen Adelman, Alon Goren, and Raul Mostoslavsky

Supplemental Figures

S1A

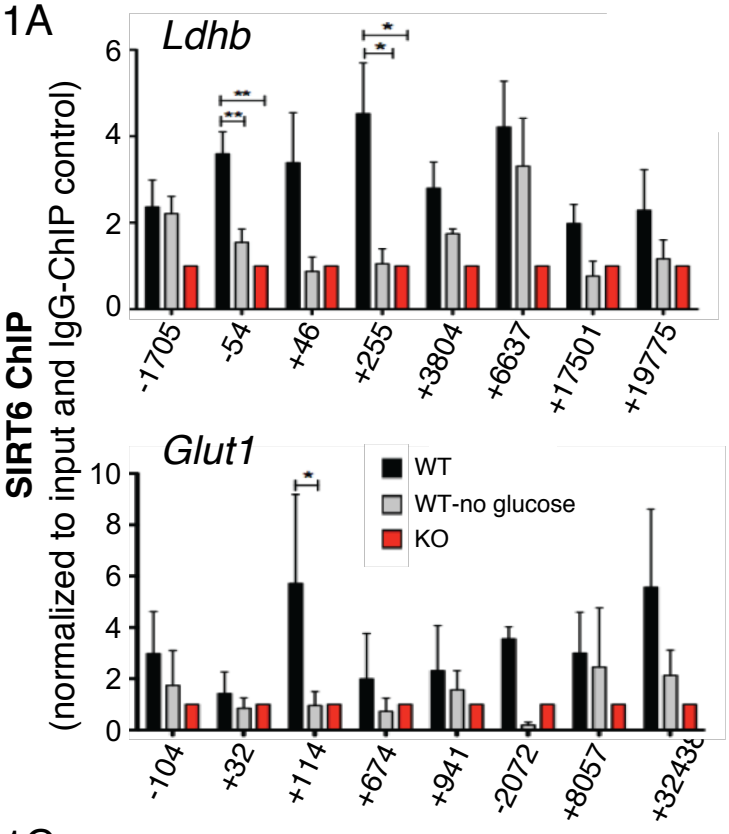

S1B

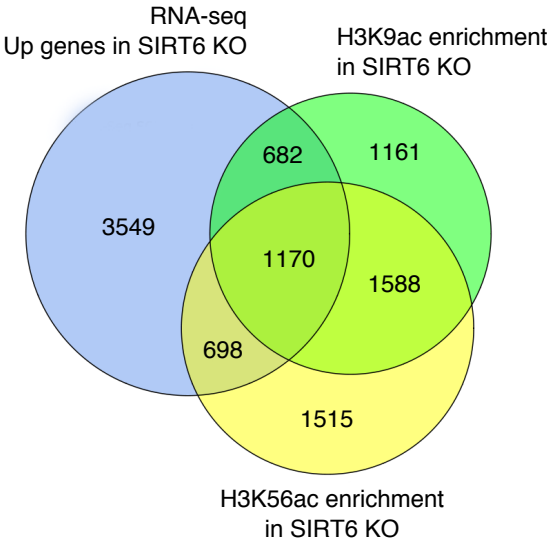

S1C

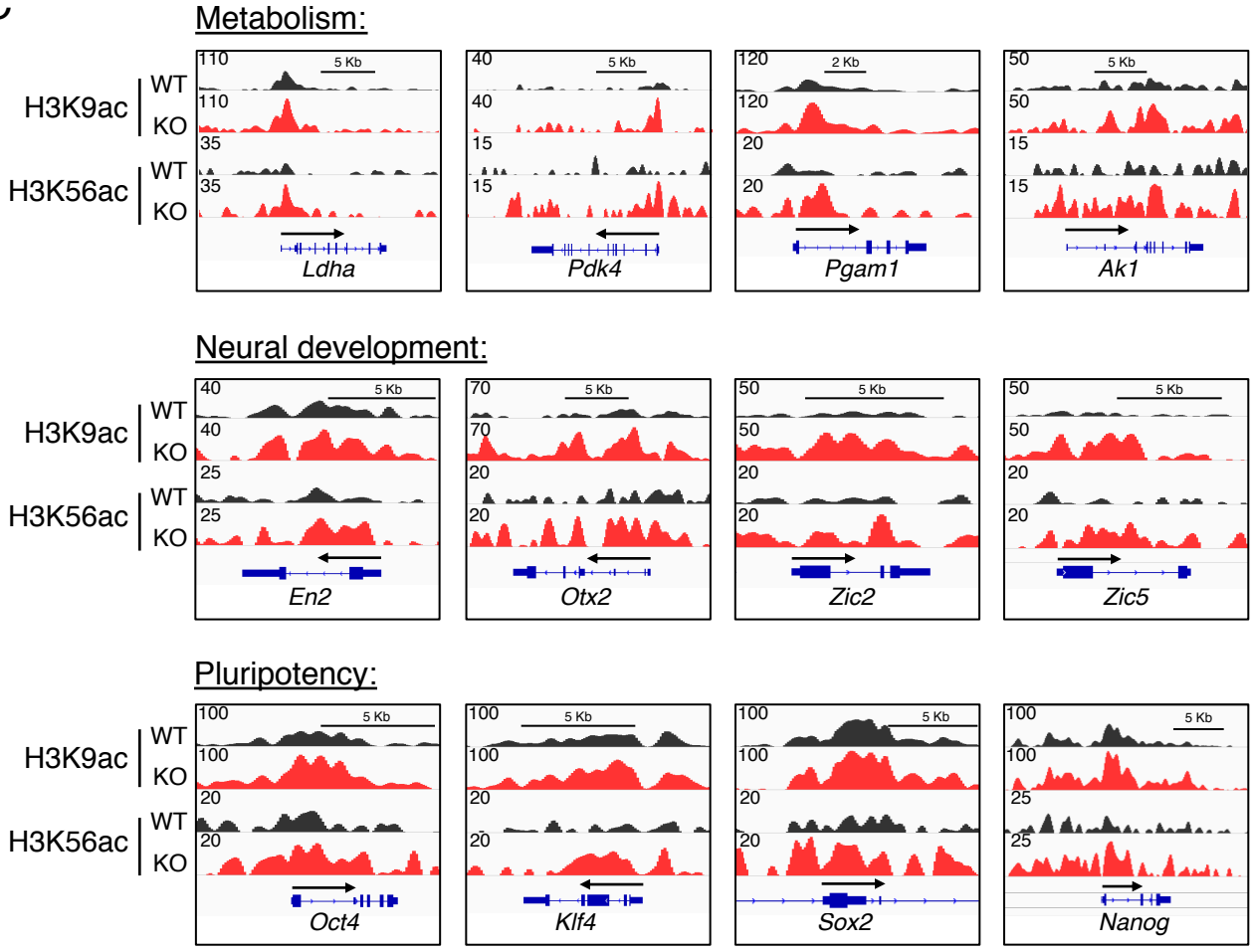

S2A

Pausing Index from Pol II ChIP-seq

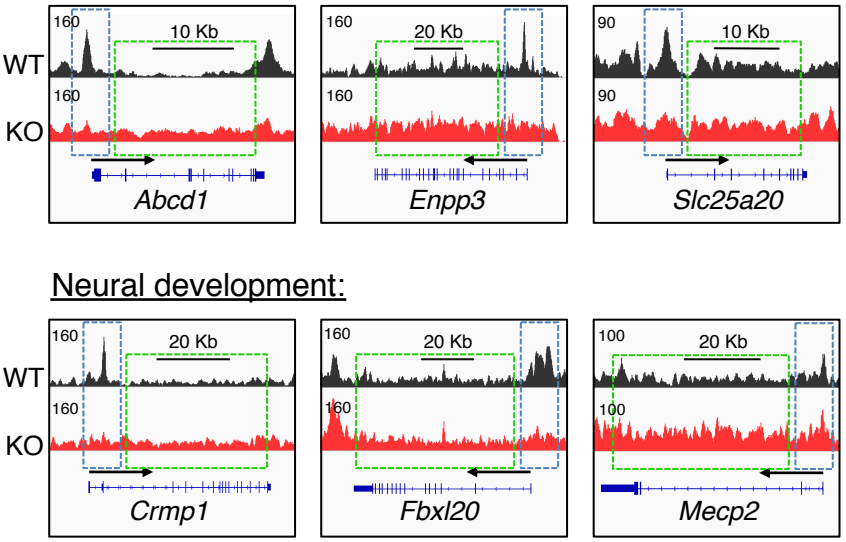

S2C

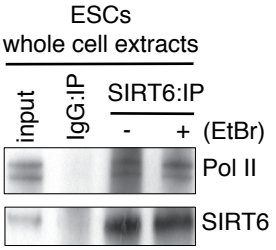

S2D

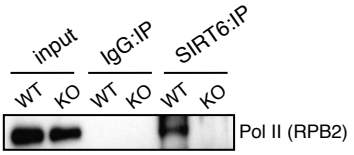

S2E

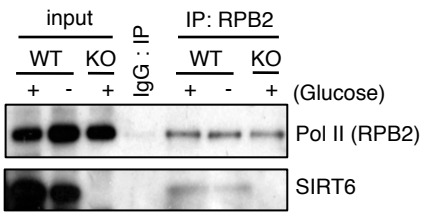

S2B

Up-regulated genes in SIRT6 KO ESCs with low Pausing Index (~2500 genes)

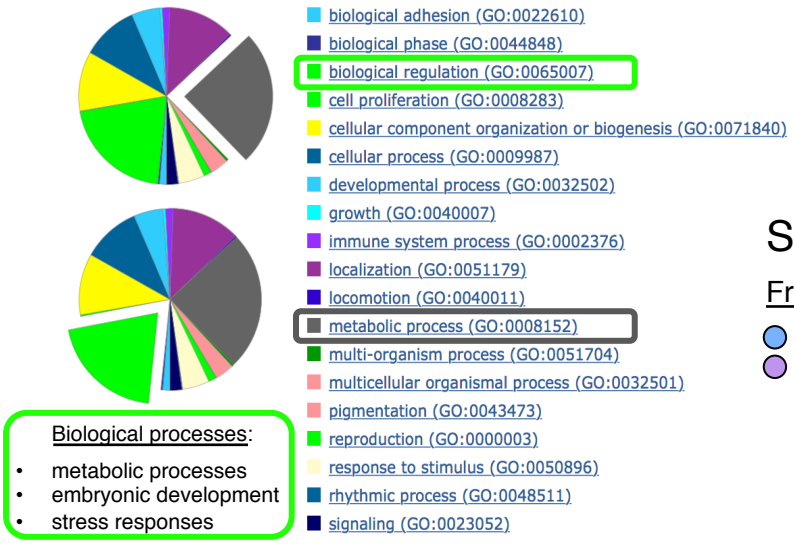

Biological processes:

- metabolic processes
- embryonic development
- stress responses

S2F

Mass spectrometry analysis

Gene	MW	Peptides (Avg=2)	P-value
RPB2	134	34	1.1E-03
Top2A	97	9	4.1E-04
Med23	174	17	6.1E-05

S2G

From Pol II ChIP-seq:

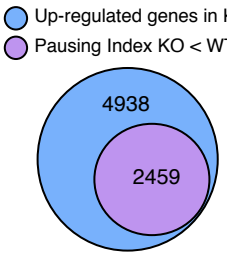

S2H

From PRO-seq:

S2I

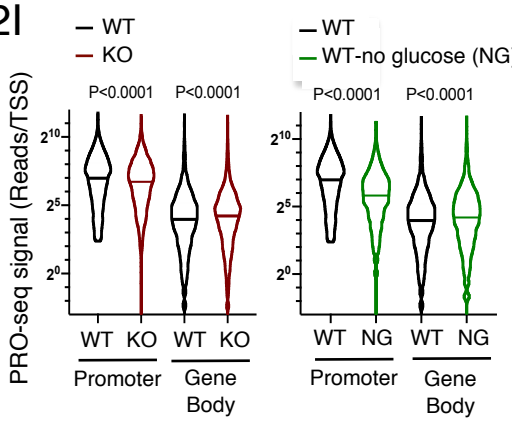

S2J

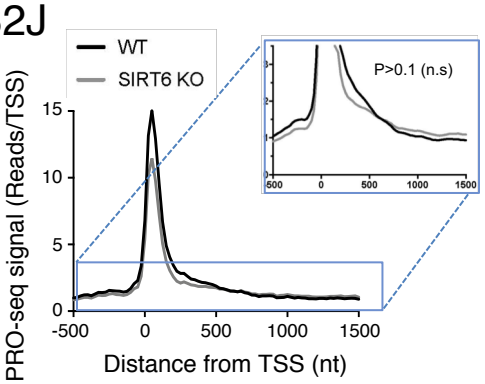

PRO-seq:
unchanged genes (N=3905)

S2K

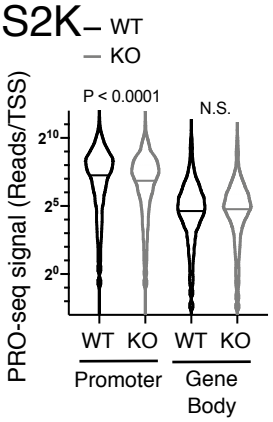

S3A

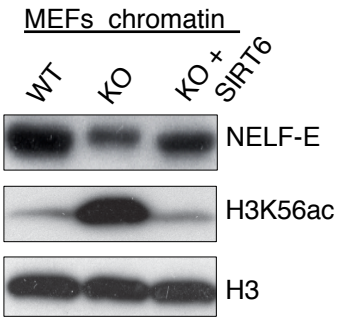

S3B

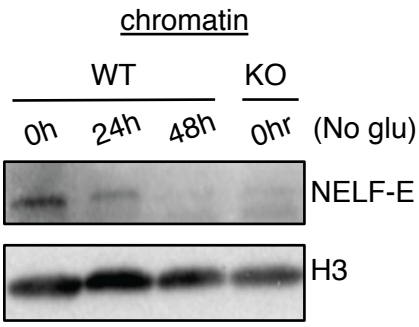

S3C

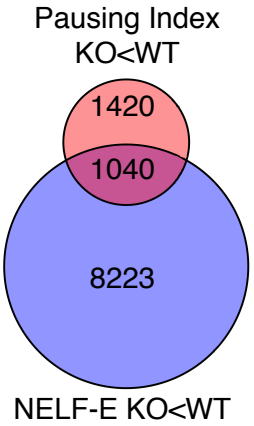

S3D

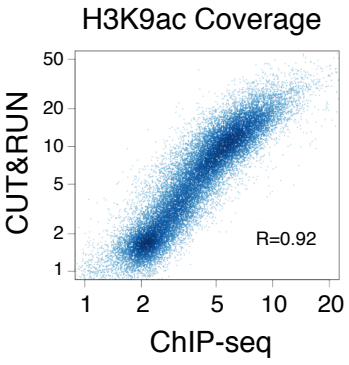

S3E

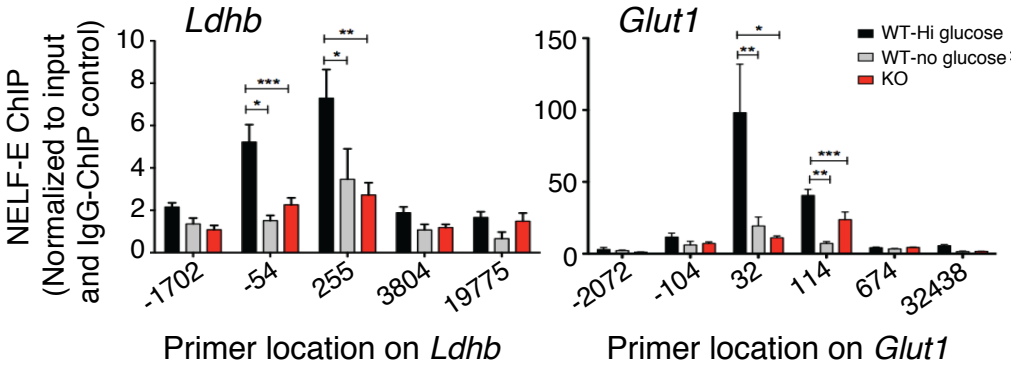

S3F

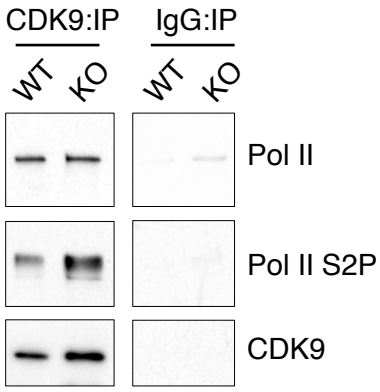

S3G

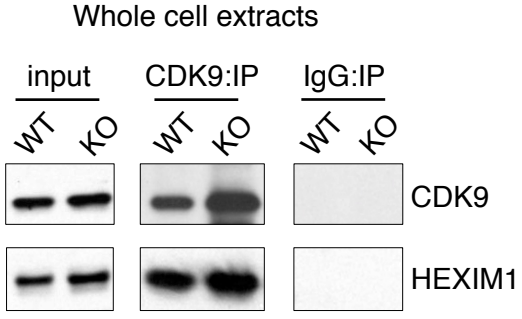

S4A

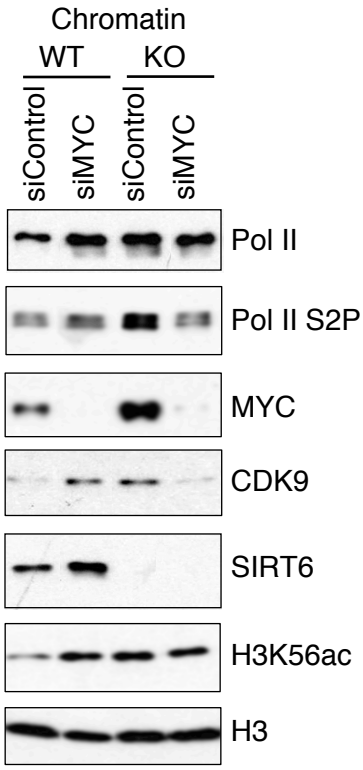

S4B

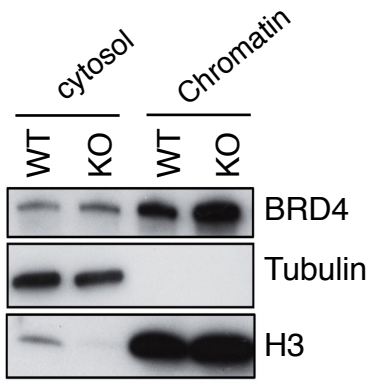

S4C

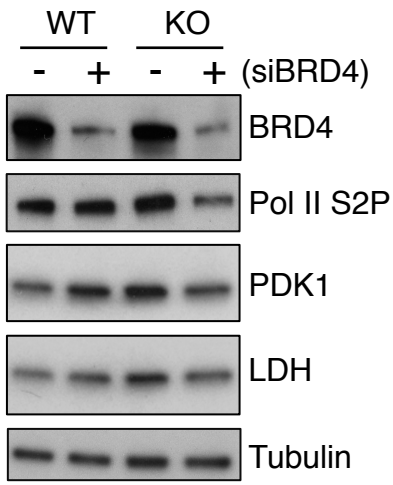

S4E

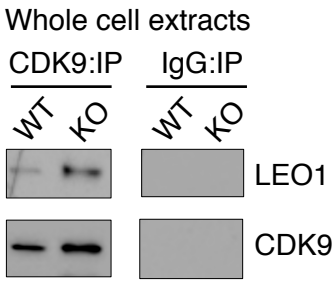

S4D

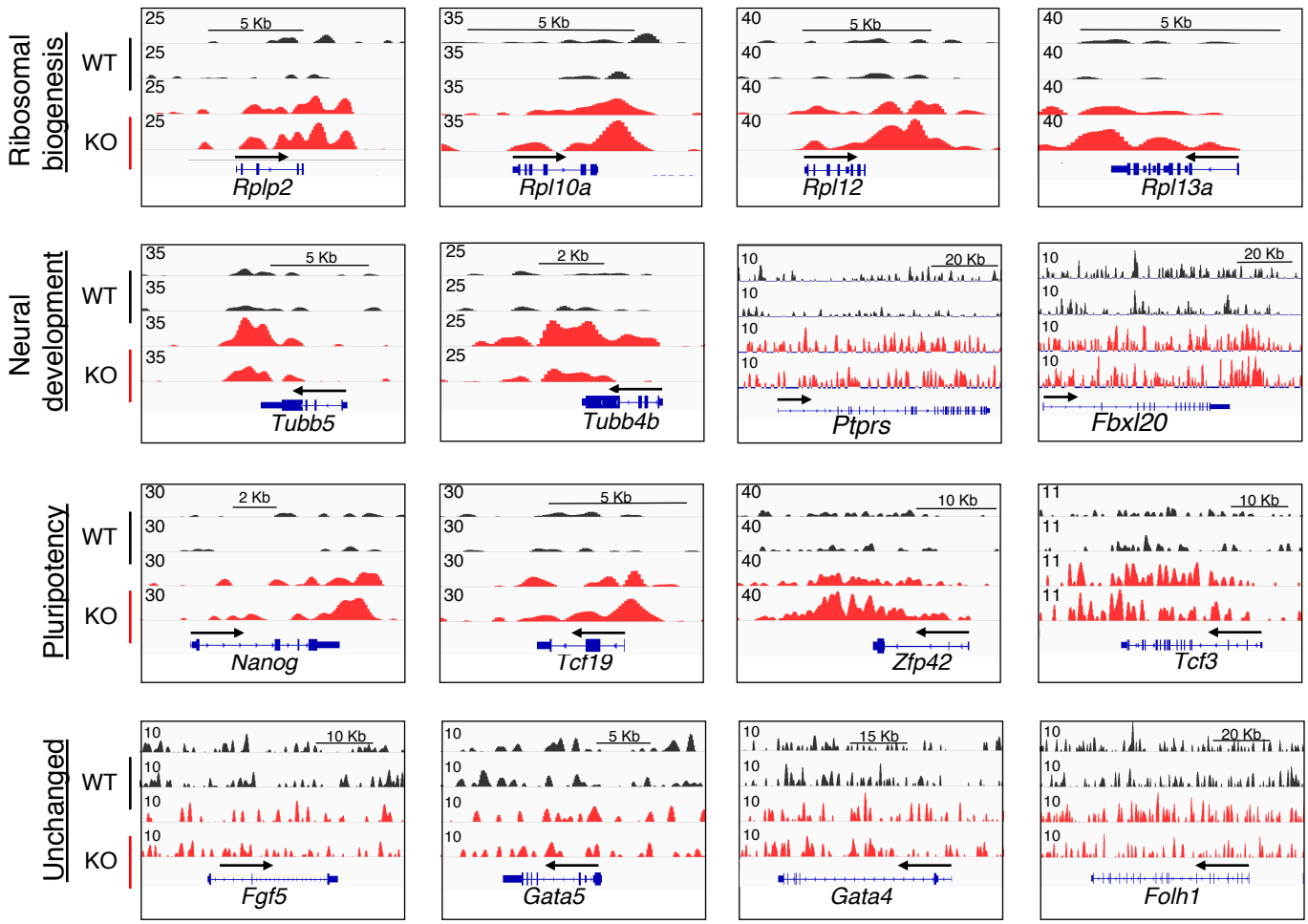

S5A

Neural development		Metabolism	
Gene	p-value	Gene	p-value
Zic22	4.7E-61	Ldhb	2.2E-34
Otx2	7.6E-92	Pfkp	1.7E-52
Zic5	7.6E-41	Idh3g	3.6E-26
Pnck	7.7E-19	Igfbp2	2.2E-30
Epha4	3.3E-29		
Ssr4	1.7E-19		
Ubac2	2.4E-24		
Pdzd4	3.0E-23		
Flna	8.4E-12		

S5B

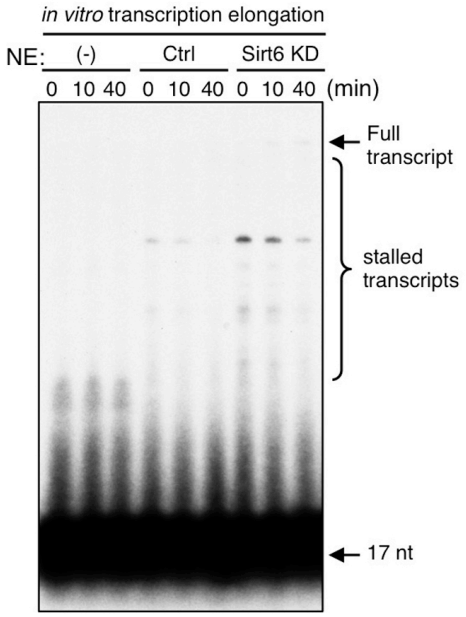

S6A

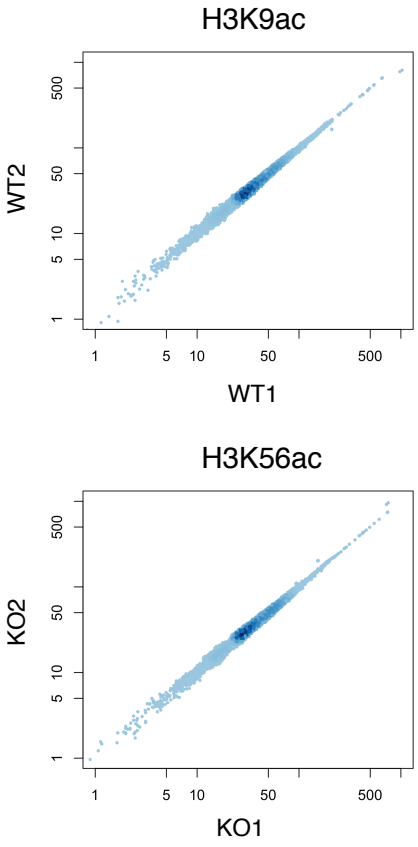

S6B

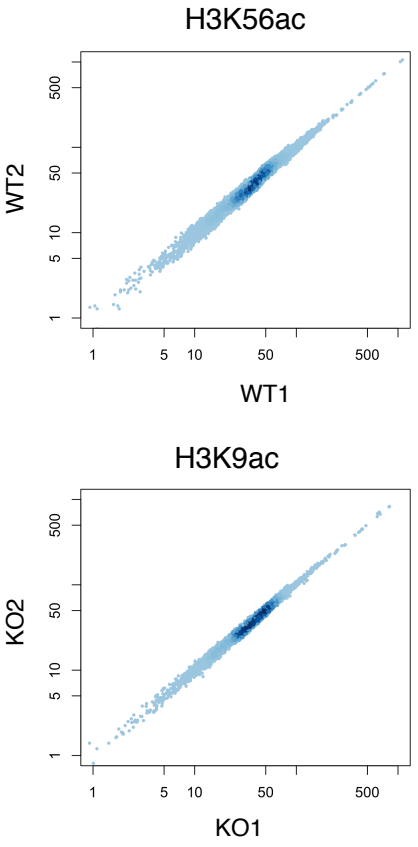

S6C

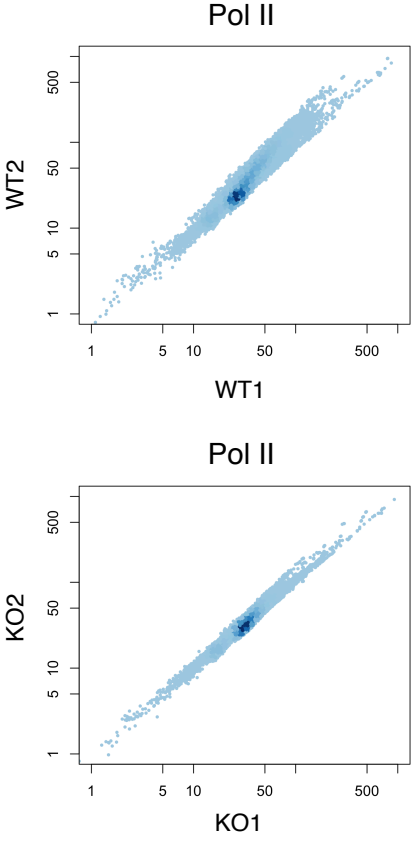

S6D

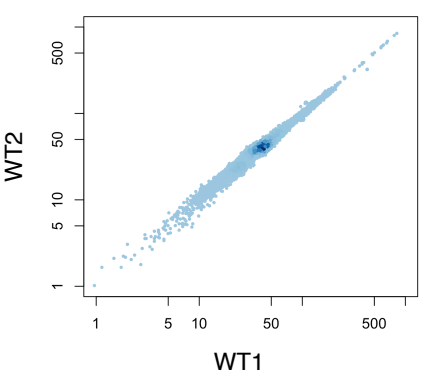

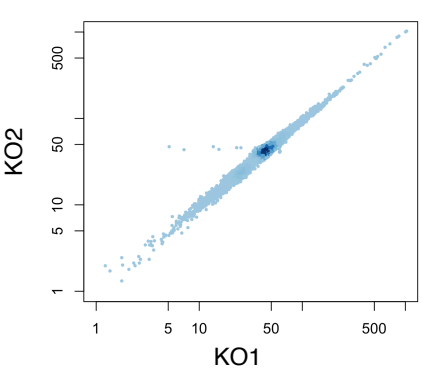

S6E

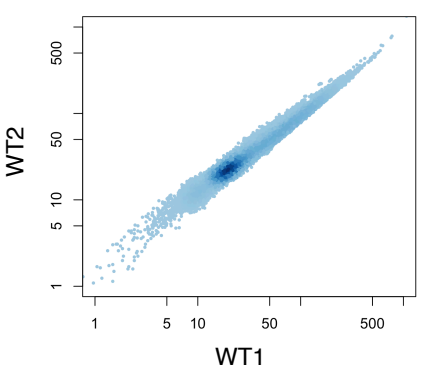

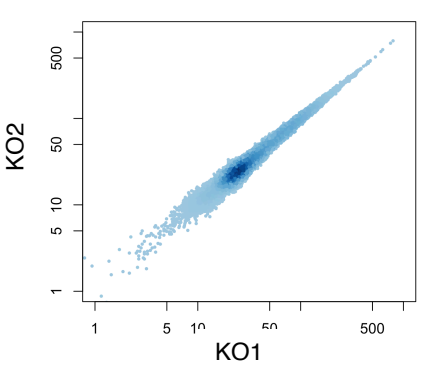

S6F

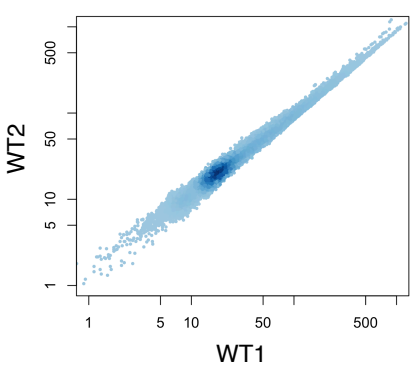

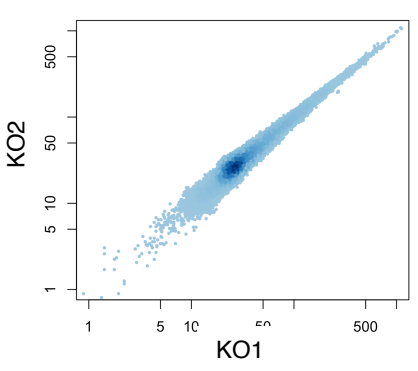

S7A

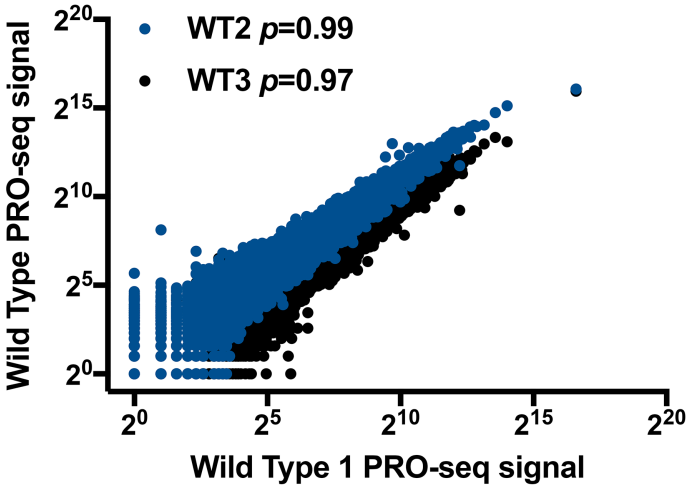
WT2 p=0.99
WT3 p=0.97
Wild Type PRO-seq signal
Wild Type 1 PRO-seq signal
2^0
2^5
2^10
2^15
2^20

S7B

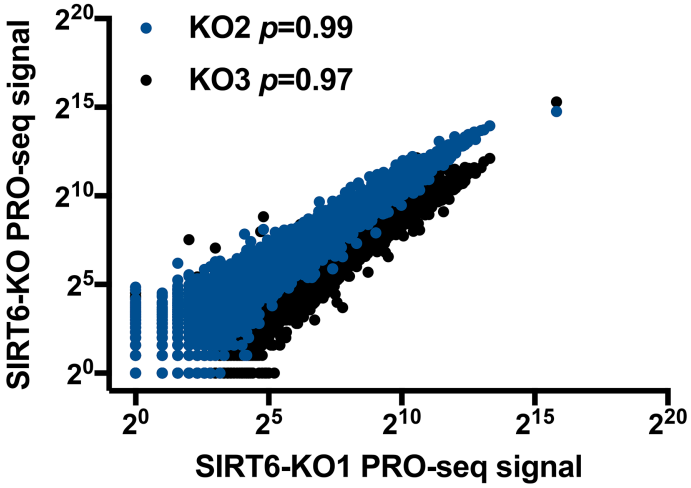
KO2 p=0.99
KO3 p=0.97
SIRT6-KO PRO-seq signal
SIRT6-KO1 PRO-seq signal
2^0
2^5
2^10
2^15
2^20

S7C

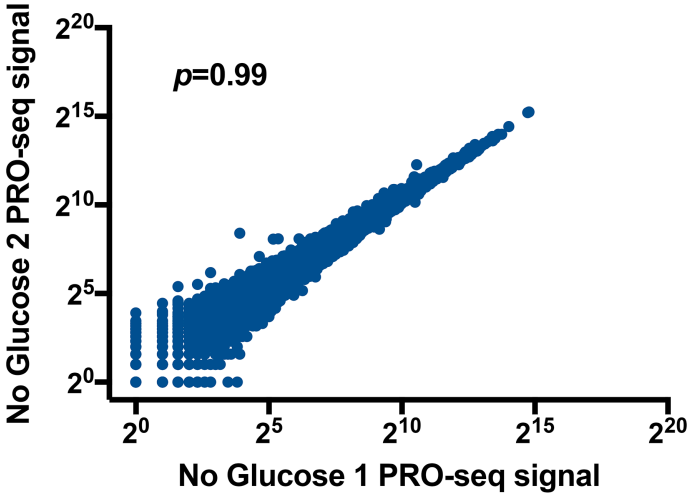
p=0.99
No Glucose 2 PRO-seq signal
No Glucose 1 PRO-seq signal
2^0
2^5
2^10
2^15
2^20

SUPPLEMENTAL FIGURE LEGENDS

Figure S1, related to Figure 1:

Figure S1A. ChIP-qPCR for SIRT6 on *Ldhb* and *Glut1* genes. Data (n=3) was normalized to input and IgG-ChIP controls. Data are presented as ratios where values from SIRT6 KO ESCs (red) are equal to 1. (*: $p < 0.05$, **: $p < 0.005$, n = 3. Error bar represents s.e.m).

Figure S1B. Venn diagram showing the overlapping between up-regulated genes in SIRT6 KO ESCs and H3K9ac/H3K56ac enriched genes in SIRT6 KO ESCs.

Figure S1C. Increased H3K9ac and H3K56ac levels in SIRT6 KO ESCs at specific genes. IGV broswer images from H3K9ac and H3K56ac ChIP-seq showing enrichment in SIRT6 KO (red) compared to WT ESCs (black) on genes involved in metabolism, neural development and pluripotency.

Figure S2, related to Figure 2:

S2A. Decreased Pol II pausing in SIRT6 KO ESCs at specific genes. IGV broswer images from elongating Pol II ChIP-seq showing increased levels in SIRT6 KO (red) *versus* WT ESCs (black) on genes involved in metabolism and neural development. **S2B.** Pie charts showing functional gene categories for the up-regulated genes in SIRT6 KO ESCs. Biological processes were determined by gene onthology analysis using Panther classification system (Thomas et al., 2003). **S2C.** Western blot showing direct interaction between endogenous SIRT6 and Pol II by co-immunoprecipitation assays using whole cell extracts from WT ESCs (+/- ethidium bromide). **S2D.** Western blot showing co-immunoprecipitation between SIRT6 and the Pol II subunit, RPB2, using nuclear extracts from WT and SIRT6 KO ESCs. **S2E.** Western blots showing co-immunoprecipitation between RPB2 and SIRT6 using nuclear extracts derived from WT, WT deprived of glucose and SIRT6 KO ESCs. **S2F.** Mass spectrometry analysis from HeLa cells overexpressing SIRT6 showing the enrichment for RPB2, TOP2A and MED23. **S2G.** Venn diagram from Pol II ChIP-seq analysis showing that nearly 50% of the up-regulated genes in SIRT6 KO ESCs have lower Pausing Index compared to WT cells. **S2H.** Venn

diagram from PRO-seq analysis showing about 75% of the up-regulated genes in SIRT6 KO ESCs have lower Pausing Index compared to WT cells. **S2I.** Biolin plots from PRO-seq analysis showing the significant decrease of Pol II levels near promoter-proximal regions in SIRT6 KO (red) and glucose starved WT (green) ESCs compared to WT (black) control cells. This plots also show a significant increase in Pol II levels at gene bodies of up-regulated genes in SIRT6 KO (red) or glucose deprived WT (green) ESCs. **S2J.** Metagene profile showing Pol II levels in unchanged genes between WT (black) and SIRT6 KO (gray) ESCs. **S2K.** Violin plots from PRO-seq analysis showing the significant decrease of Pol II levels near promoter-proximal regions in unchanged genes between SIRT6 KO (gray) and WT (black) ESCs. However, there is no significant changes in Pol II levels at gene bodies in these genes.

Figure S3, related to Figure 3:

S3A. Western blots showing the ectopic expression of SIRT6 rescues the decrease in chromatin-bound NELF-E in SIRT6 KO ESCs. **S3B.** Western blots showing levels of NELF-E and histone H3 in WT ESCs at various time-points after glucose starvation, and SIRT6 KO ESCs. **S3C.** Venn diagram showing the overlap between genes that demonstrate a reduction in Pausing Index and the levels of NELF-E binding in ESCs lacking SIRT6. **S3D.** Scatter plot showing high level of association between CUT&RUN and ChIP-seq data for H3K9ac. **S3E.** Decreased localization of NELF-E near pausing sites on SIRT6 target genes in both SIRT6 KO and WT ESCs grown under conditions of glucose starvation. NELF-E ChIP-qPCR on *Ldhb* or *Glut1* genes in WT ESCs grown in normal conditions (high glucose; black) or under glucose starvation (low glucose; grey), and in SIRT6 KO ESCs grown in normal levels of glucose. Data was normalized to input and IgG ChIP control. Error bars represents s.e.m (*: $p < 0.05$, **: $p < 0.01$, ***: $p < 0.001$, $n = 3$). **S3F.** Western blots showing co-immunoprecipitation of CDK9 with Pol II and Pol II Ser2P.

Figure S4, related to Figures 4-6:

S4A. Western blot analysis showing decreased levels of Pol II Ser2P and CDK9 in chromatin fractions from SIRT6 KO ESCs after acute siRNA-mediated depletion of MYC. **S4B.** Western blots showing increased levels of BRD4 in chromatin, but not cytosolic fractions from SIRT6 KO *versus* WT ESCs. **S4C.** Western blots showing the rescue of PDK1 and LDH up-regulation upon siRNA-dependent depletion of BRD4 in SIRT6 KO ESCs. **S4D**. Increased recruitment of the PAF1 complex subunit LEO1 in SIRT6 KO ESCs at specific genes. IGV browser images from LEO1 ChIP-seq in SIRT6 KO (red) *versus* WT ESCs (grey) on genes implicated in metabolism, ribosomal biogenesis, neural development and pluripotency. IGV browser images of genes with no differences in LEO1 levels between WT and SIRT6 KO ESCs are included as controls.

Figure S5, related to Figure 7:

S5A. List of genes enriched for H3K9ac, H3K56ac, H3K36me3 and H3K79me2. These genes are exclusively involved in metabolism and neural development. **S5B.** Lower exposure film of the *in vitro* transcription elongation assay in Figure 7G.

Figure S6, related to Methods (Chip-Seq analysis):

Pearson Correlation plots for ChIP-seq in WT and SIRT6 KO ESCs (n=2): (A) H3K9ac, (B) H3K56ac, (C) Pol II, (D) LEO1, (E) H3K36me3, (F) H3K79me2. Pearson R between replicates were calculated by covering over 10Kb windows across the genome.

Figure S7, related to Methods (Genomic Statistical tests):

A-C. Correlation plots from PRO-seq analysis between WT (S7A), SIRT6 KO (S7B) and glucose starved WT (S7C) ESCs. Spearman correlations (ρ) were calculated by using a +/- 250bp window around promoters (N=17032) of annotated genes for each of the replicates in WT, WT No Glucose or SIRT6-KO conditions.